

EUROPE'S 2003 HEAT WAVE: A SATELLITE VIEW OF IMPACTS AND LAND–ATMOSPHERE FEEDBACKS

BENJAMIN F. ZAITCHIK,^{a,*} ALISON K. MACALADY,^b LAURENT R. BONNEAU^c and RONALD B. SMITH^d

^a *Department of Geology and Geophysics, Yale University, USA*

^b *School of Forestry and Environmental Studies, Yale University, USA*

^c *Center for Earth Observation, Yale University, USA*

^d *Department of Geology and Geophysics, Yale University, USA*

Received 20 March 2005

Revised 27 September 2005

Accepted 28 September 2005

ABSTRACT

A combination of satellite imagery, meteorological station data, and the NCEP/NCAR reanalysis has been used to explore the spatial and temporal evolution of the 2003 heat wave in France, with focus on understanding the impacts and feedbacks at the land surface. Vegetation was severely affected across the study area, especially in a swath across central France that corresponds to the Western European Broadleaf (WEB) Forests ecological zone. The remotely sensed surface temperature anomaly was also greatest in this zone, peaking at +15.4 °C in August. On a finer spatial scale, both the vegetation and surface temperature anomalies were greater for crops and pastures than for forested lands. The heat wave was also associated with an anomalous surface forcing of air temperature. Relative to other years in record, satellite-derived estimates of surface-sensible heat flux indicate an enhancement of 48–61% (24.0–30.5 W m⁻²) in WEB during the August heat wave maximum. Longwave radiative heating of the planetary boundary layer (PBL) was enhanced by 10.5 W m⁻² in WEB for the same period. The magnitude and spatial structure of this local heating is consistent with models of the late twenty-first century climate in France, which predict a transitional climate zone that will become increasingly affected by summertime drought. Models of future climate also suggest that a soil-moisture feedback on the surface energy balance might exacerbate summertime drought, and these proposed feedback mechanisms were tested using satellite-derived heat budgets. Copyright © 2006 Royal Meteorological Society.

KEY WORDS: remote sensing; heatwave; drought; climate change; land–atmosphere feedback; surface energy balance

1. INTRODUCTION

The European heat wave of the summer of 2003 was an extreme climatic anomaly: the mean summertime temperatures over much of western and central Europe exceeded the 1961–1990 mean by up to 5 standard deviations, and the summer might have been the warmest since 1540 (Beniston, 2004; Schär *et al.*, 2004). Excessive heat and/or lack of water resulted in lower yields of grains, vegetables, fruits, and wines by between 4.6 and 10.8%, with uninsured crop losses totaling about US\$12.3 billion (INSEE, 2004; Schär and Jendritzky, 2004). In France alone, officials estimated that wheat and corn harvests decreased by 15 and 28%, respectively, with losses totaling between US\$1.1 and \$4.4 billion (Housego, 2003).

Beyond its immediate impact, the 2003 heat wave has been interpreted by many as a harbinger of long-term climate change. This interpretation is supported by simulations of future climate performed with regional climate models (RCM) forced by the IPCC B2 and A2 emission scenarios (822 and 1143 ppmv CO₂, plus sulfate forcing, respectively). Using the Rossby Center coupled RCM (RCAO), Räisänen *et al.* (2004) predict that warming in central and southern Europe will be greatest during summer, with mean summertime

* Correspondence to: Benjamin F. Zaitchik, Department of Geology and Geophysics, Yale University PO Box 208109, New Haven, CT 06520, USA; e-mail: benjamin.zaitchik@yale.edu

temperature in France 6–10 °C warmer in the late twenty-first century than it is today (for scenarios B2 and A2) and precipitation also greatly reduced. Climate models also predict an increase in climate variability associated with greenhouse-gas forcing, causing extreme events like that observed in 2003 to become more frequent in the future (Meehl and Tebaldi, 2004). On the basis of a statistical analysis of A2-forced model simulations, Schär *et al.* (2004) conclude that summers as warm as or warmer than 2003 may occur as often as every second year by the end of the century.

Models of future climate also provide predictions regarding the mechanisms responsible for producing extreme heat waves. For Europe, one important mechanism involves drought (Räisänen *et al.*, 2004). In this scenario, lack of precipitation and high temperatures combine to dry the soil, which in turn influences the partitioning of energy at the land surface. Latent heat flux (evapotranspiration) decreases, whereas sensible heat flux – which contributes directly to the warming of the near-surface atmosphere – increases. In RCM simulations for both B2 and A2 scenarios, the decrease in soil moisture is greatest in late summer, with a corresponding increase in sensible heat flux of about 40–80% (20–40 W m²) in July and August, averaged over France and calculated relative to the current climate (Räisänen *et al.*, 2004).

In addition to heating the near-surface atmosphere, a shift from latent to sensible heat flux may be associated with a reduction in the total turbulent energy transfer from the surface into the planetary boundary layer (PBL): a dry surface heats up more quickly than a moist surface, causing an increase in the longwave radiative flux from the surface and a reduction in the net radiation available at the surface (Eltahir, 1998). Assuming a surface energy balance, this decrease in net radiation causes an equivalent decrease in fluxes of energy away from the surface. The combination of enhanced sensible heat flux, which deepens the PBL (Betts and Ball, 1998), and reduced total energy transfer to the atmosphere may decrease the likelihood of convective precipitation (Small and Kurc, 2003). The result is a soil-precipitation feedback loop that tends to extend and intensify drought conditions.

In RCM simulations of Europe performed by Schär *et al.* (1999), the surface forcing on climate was found to be most active in a 1000-km wide strip located between the perennially dry Mediterranean (MED) climate zone in the south and the temperate Atlantic-influenced climate zone to the north. This ‘transitional’ climate zone was particularly sensitive to the soil moisture status: when the model was forced with a dry soil, surface changes in surface energy partitioning led to a significant reduction in summertime precipitation. Over the course of the twenty-first century, the MED climate zone is predicted to encroach northward, bringing more frequent summertime drought to this transitional climate zone and, perhaps, triggering an aridifying soil-moisture precipitation feedback (Schär *et al.*, 1999; Räisänen *et al.*, 2004).

In this paper, remotely sensed data from France, coupled with data from weather stations and an existing land-cover classification system, are used to describe the heat wave of 2003 in terms of changes in summer vegetation, surface temperature, and energy balance. This new description is then used to compare the event with RCM simulations of extreme future heat waves in western Europe. If the 2003 heat wave is truly analogous to these model-predicted extreme heat waves of the late twenty-first century, one would expect to find evidence of a significant enhancement in sensible heating that corresponds in timing and location to that invoked by RCM simulations. Observationally, this would require that (i) the heat wave was accompanied by a significant drought, (ii) the drought resulted in enhanced sensible heat flux in the affected area, and (iii) this surface forcing corresponded geographically to that revealed in the RCM simulations. If a precipitation feedback were also active, then one would expect systematic changes in net radiation or surface energy partitioning in this same transitional zone.

In addition to providing an observational test to RCM model predictions at the mesoscale, the following possibilities were investigated: (i) impacts of the heat wave were not evenly distributed across finer-scale variations in land cover and (ii) different land-cover types had a differential effect on land surface feedbacks on air temperature during the event.

Thematically, the paper proceeds from heat wave impacts to land–atmosphere feedbacks. Structurally, it begins with an inventory of datasets and processing techniques (Section 2), followed by an analysis of impacts on vegetation and surface temperature (Section 3). In Section 4, the 2003 anomalies in the surface radiation and energy budgets are summarized, leading to an investigation of local feedbacks on temperature (Section 5)

and the potential for a drought–precipitation feedback (Section 6). In Section 7 a summary and conclusions are presented.

2. DATASETS AND DATA PROCESSING

2.1. Satellite imagery

Remotely sensed imagery for this study comes from the MODerate Imaging Spectrometer (MODIS) and Advanced Spaceborne Thermal Emission and Reflection Radiometer ASTER sensors aboard the Terra satellite. Each set of images, along with spatial and temporal resolutions, coverage dates, and basic quality control (QC) preprocessing techniques, is listed in Table I.

After checking QCs (Table I), a time series of images were constructed for each of the MODIS composite products listed in Table I. This time series runs from April to mid-October (Julian dates 97–288) for every year in which MODIS images were available (2000–2004). From this data, a '2003 anomaly' was created for each of the composite periods. The 2003 anomaly was calculated by taking the difference between the 2003 value and the mean of the 2000, 2001, 2002, and 2004 values (hereafter the 'MODIS era baseline'), and was calculated on a pixel-by-pixel basis.

To facilitate the analysis of land-cover controls on the surface energy budget, a pair of high-resolution ASTER images from 1 August 2000 and 10 August 2003 were selected. There was a significant rainfall event 1 week prior to the 2000 acquisition date and trace rain just two days before the image was acquired. There was no recorded rainfall in the week preceding the 2003 image. While the difference in rainfall and image date means that the pair does not offer a perfect comparison, the rainfall events preceding the 2000 acquisition date were not atypical of summertime storms in the region.

2.2. Ancillary data

Daily records of precipitation, mean 2-m winds, and 2-m air temperature (mean, maximum, and minimum) from Climate Diagnostic Center archive of meteorological station records were used to construct an air temperature time series for all of France and to perform flux calculations at ASTER scale. A total of 126 stations in France reported a continuous data record between April 2000 and October 2004. Incoming radiation fluxes were obtained from the NCEP/NCAR reanalysis 6-hourly data archive (Kalnay *et al.*, 1996), as were winds and air temperature at $\sigma = 0.995$ (approximately 40 m height). The reanalysis data are appropriate for MODIS-scale application under the assumptions that incoming radiation is relatively uniform over a $2^\circ \times 2^\circ$ reanalysis grid cell when averaged over 8 or 16 days and that 40 m is a reasonable 'blending' height over the same averaging period.

Variability in heat wave impacts and energy fluxes across geographic regions in France is considered in the context of the major European ecological regions, as defined by the European Environment Agency (Figure 1). The transitional climate zone described by Schär *et al.* (1999) corresponds closely to the 'Western European Broadleaf (WEB) Forests' ecological region. This region lies between MED and highland (Alps (ALP) and Pyrenees) climate zones to the south and the southern temperate Atlantic (ATL) zone to the north. These ecological zones are defined on the basis of climate, topography, and potential vegetation (Bonn, 1994), and are best interpreted as areas of relatively homogeneous ecological conditions (Painho, 1996). While the European Environment Agency (EEA) defines five major ecological regions in France (southern temperate ATL, WEB Forest, MED, ALP and Pyrenees), the present analyses are focused largely on the southern temperate ATL, WEB, and MED zones, as they constitute most of the land area and include almost all of France's agricultural lands (Figure 1, Table II).

The land-cover analysis is aided by the CORINE Land Cover classification developed by the European Commission program to COoRdinate INformation on the Environment (Heymann *et al.*, 1993). For simplicity of presentation, land-cover results are expressed in terms of a subgrouping of the 44 classes in the CORINE product. The classes for 'nonirrigated agriculture' and 'complex cultivation' (heterogeneous area dominated

Table I. Description of satellite data products and quality control preprocessing used in this study

Sensor	Product name	Product ID	Spatial resolution	Temporal resolution	Coverage dates	Product data layers utilized
MODIS Terra	Vegetative indices	mod13q1	250-m	16-day composite ^d	April–October (JD 97–288), 2000–2004	NDVI, Quality control (QC) flags ^a
MODIS Terra	Land surface temperature (LST) and thermal emissivity	mod11a2	1-km	8-day composite ^d	April–October (JD 97–288), 2000–2004	Day and night-time radiometric LST (approximately 10 a.m. and 10 p.m. overpass time), band 31 surface emissivity, QC flags
MODIS Terra	Bidirectional reflectance distribution function-corrected surface albedo	mod43b3	1-km	16-day composite ^d	April–October (JD 97–288), 2000–2004	Broadband white-sky albedo (bihemispherical reflectance) for the visible and near infrared ^b
MODIS Terra	Atmospherically corrected surface reflectances	mod09ghk	500-m	Daily	1 August 2000 and 10 August 2003	Band 1 and 2 (620–670 nm, 841–876 nm), QC flags
MODIS Terra	Land surface temperature (LST) and thermal emissivity	mod11a1	1-km	Daily	1 August 2000 and 10 August 2003	Day and night-time radiometric LST (approximately 10 a.m. and 10 p.m. overpass time), band 31 surface emissivity, QC flags
ASTER Terra	Atmospherically corrected surface reflectances	AST_03	15-m	Single day	1 August 2000 and 10 August 2003	Bands 1, 2, 3 (520–600 nm, 630–690 nm, 780–860 nm)
ASTER Terra	Atmospherically corrected surface albedo	AST_04	15-m	Single day	1 August 2000 and 10 August 2003	Broadband white-sky albedo (bihemispherical reflectance) for the visible and near infrared
ASTER Terra	Kinematic surface temperature	AST_07	90-m	Single day	1 August 2000 and 10 August 2003	1 temperature band ^c

^a MODIS products are distributed with missing or corrupt data replaced with a null value. The present study used QC flags to identify potential snow and ice cover in the *NDVI* composites and to flag potential cloud-edge and thin cloud influence on reported land surface temperature. These data were eliminated from the calculations.

^b White-sky albedo is calculated under the assumption of an isotropic diffuse radiation field and is equivalent to the hemispheric integral of direct albedo (Schaaf *et al.*, 2002).

^c AST-07 product algorithms are described in Gillespie *et al.*, 1998.

^d The MODIS compositing procedure is designed to minimize the influence that clouds and other atmospheric abnormalities have on the estimation of surface properties (Vermote and Vermeulen, 1999). The *NDVI* composite consists of the maximum daily *NDVI* value recorded with good quality at each pixel in the 16-day compositing period (Huete *et al.*, 1999). The land surface temperature composite uses an average of all clear-sky measurements obtained during the compositing period. The BRDF-corrected albedo composite takes advantage of multiple clear-sky looks to solve the bidirectional reflectance distribution function (Schaaf *et al.*, 2002).

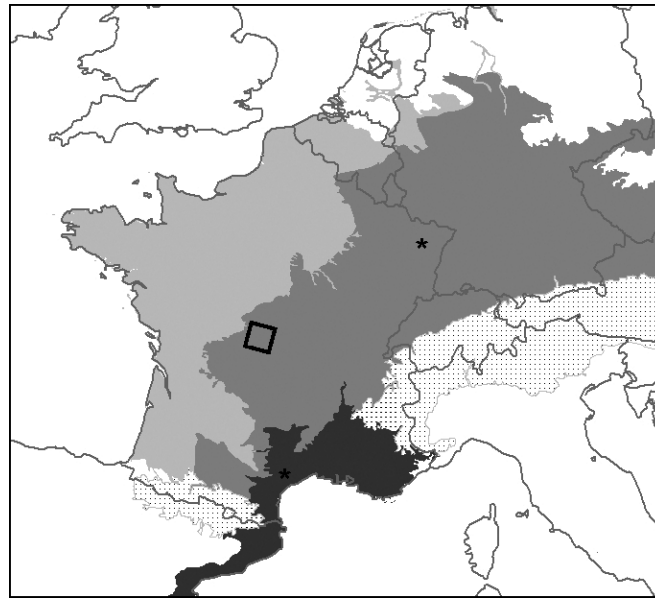


Figure 1. Dominant ecological zones of France – Mediterranean (dark gray) Western European Broadleaf Forests (medium gray), southern temperate Atlantic (light gray), and Alps and Pyrenees highland zones (striped). The black box shows the footprint of the ASTER image pair and stars are locations of Euroflux sites: Puechebon in the Mediterranean zone and Hesse Forest in the zone of western European Broadleaf Forests. Ecozone map European Environmental Agency, Copenhagen, 2000

Table II. Total area and average elevation of land-cover types within the three major ecozones and for all of France. Area is in km² and elevation is meters

Land cover	Mediterranean		W. Eur. Broadleaf		Temperate Atlantic		Alps		All of France	
	Area	Elevation	Area	Elevation	Area	Elevation	Area	Elevation	Area	Elevation
Crops	10 273	381	69 271	293	137 981	110	1 072	723	196 412	186
Pastures	1 280	633	45 060	447	32 911	116	985	1 001	70 663	327
Broadleaf and mixed forests	16 300	581	47 659	431	31 429	142	2 597	1 022	103 046	408
Coniferous forests	3 298	821	13 256	728	14 466	83	3 237	1 454	43 838	557
Orchards	8 019	122	1 479	258	4 396	76	46	355	11 729	124
Urban	1 461	163	6 062	294	11 503	73	398	683	24 613	164
Other	16 776	646	16 003	544	16 790	111	9 399	2 075	87 306	740
All	57 408	504	198 790	410	249 475	111	17 733	1 630	537 606	365

by agriculture) are combined into a single ‘nonirrigated crops’ class for time-series analyses. The ‘deciduous’ and ‘coniferous’ forest classes are reported separately when there was a systematic difference between them, but are combined with the CORINE ‘mixed’ forest class into a general ‘forest’ category when the response of all forest types was similar. Results for pastures reflect values from only the CORINE pasture class. As the resolution of the ASTER image was significantly greater than that of the CORINE land-cover database, forest, cropped land, pasture, and urban land-cover classes within the ASTER image were defined by supervised classification performed with ER Mapper 6.4 image processing software (Earth Resource Mapping Ltd.).

Elevation data, used as a control on variability in the analysis of MODIS-derived vegetation index and surface temperature during the heat wave, were obtained at 90-m horizontal resolution from the Shuttle Radar Topography Mission (SRTM) global dataset (Farr and Kobrick, 2001).

3. IMPACTS ON THE LAND SURFACE: DROUGHT AND PROLONGED HEAT

In this section, basic documentation of the spatial and temporal aspects of the 2003 heat wave are provided in terms of two remotely sensed variables important to understanding land–atmosphere interactions – vegetation and surface temperature. Across the domain, vegetative conditions during the heat wave are described in terms of a common remotely sensed vegetative index, the MODIS normalized difference vegetation index (*NDVI*), and surface temperature is measured in terms of MODIS-based radiometric temperature (T_R). To get a better sense of differences between land-cover types, *NDVI* and T_R are looked at with much higher spatial resolution using images from the ASTER sensor.

3.1. Vegetation

Vegetation plays an important role in regulating energy, water, and carbon exchanges between the land surface and the atmosphere. On shorter timescales, plants opening or closing their stomata exert control over transpiration and the partitioning of energy at the surface (Chen *et al.*, 2001). The timing of plant leaf-out in spring and senescence in fall influences the hydrologic cycle and carbon uptake on a seasonal timescale (Bounoua *et al.*, 2000; Stöckli and Vidale, 2004), and the spatial extent and pattern of different vegetative cover types influence energy and momentum fluxes on even longer timescales (Pielke and Avissar, 1990).

Satellite-derived *NDVI* can be used to monitor vegetation and its influence on these exchanges. Change in *NDVI* reflects changes in the condition of vegetation, and is often used as a simple proxy for changes in ecologically important variables such as the fraction of photosynthetically active radiation (fPAR) and the leaf area index (LAI) (Asrar *et al.*, 1984, 1985a, b; Myneni and Williams, 1994; Rasmussen, 1998; Veroustraete *et al.*, 2002). Because these parameters respond strongly to precipitation in the preceding days and months (Tucker *et al.*, 1986), change in *NDVI* is widely used as an indicator of moisture stress and drought (Kogan, 1995, 1997; Liu and Kogan, 1996; Peters *et al.*, 2002; Ji and Peters, 2003; Wan *et al.*, 2004).

An analysis of the MODIS *NDVI* time series in the present study reveals a distinct spatial and temporal signature to the vegetative growth and stress during the 2003 growing season, with an anomalously early green-up in the spring of 2003 and severe vegetative stress later in the summer (Figures 2 and 3). A positive late-April *NDVI* anomaly (*NDVI'*) existed across all ecological zones and was probably a response to early spring warmth. However, a negative *NDVI'* began to develop by June, first in the WEB zone (on both an absolute and percentage basis), and then progressively later in MED, ATL and the ALP. By July and August, *NDVI* values had dropped precipitously across the study area.

Compared to the MODIS era baseline, *NDVI* values at the height of the 2003 heat wave (mid-August) were on average 0.1 – or about 15% – lower across the study area, with both the earliest and greatest reductions in *NDVI* occurring in the WEB ecological zone. A Welch ANOVA test for unequal variances on a subset of the *NDVI'* data ($n = 4857$, sampled across France at 10 km intervals) confirms that the difference between *NDVI'* in ATL, ALP, WEB and MED is statistically significant throughout the season, with F -values ranging from 27.40 in early April to 103.73 in mid-August (P -values all < 0.0001) (Figure 3(B)). Distribution of *NDVI* values also differs across years, with standard deviations generally increasing in 2003 *versus* the MODIS era baseline, especially in WEB and for forest land-cover classes.

To give a sense of the absolute variability in *NDVI* between years, Figure 4 shows the complete MODIS *NDVI* time series from April to October in 2000–2004 for each ecological zone. *NDVI* values are generally higher in the WEB zone than in ATL, MED, or ALP, but all regions show a severe decline in *NDVI* in July and August 2003 as compared to the seasonal sequence in other years. Figure 4 captures several other important features including the difference in phenology between the high altitude ALP zone and the other regions (although some of this effect may be due to remaining snow in the Alpine zone rather than delay of green-up) and the recovery of *NDVI* in September 2003.

At a finer spatial scale, the heat wave had significantly different effects on different land-cover types. A negative *NDVI'* developed earlier and became more severe in pastures and croplands as compared to *NDVI'* for forests, on both an absolute and a percentage basis (Figure 5 for absolute *NDVI'*). Across France, the relationship between *NDVI'* and land cover is strongest at the height of the heat wave, represented by the

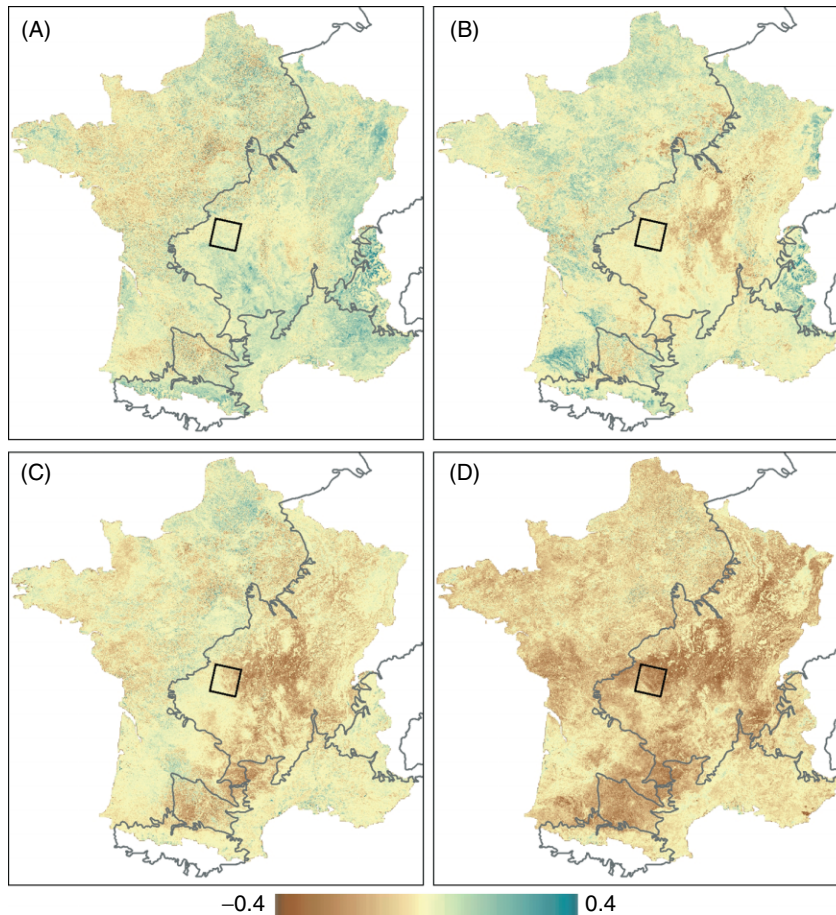


Figure 2. 2003 $NDVI$ anomaly ($NDVI'$, unitless) calculated from MODIS 16-day composites for (A) 23 April–8 May, (B) 10–25 June, (C) 12–27 July and (D) 13–28 August. Ecological zones are outlined in gray; the ASTER footprint is indicated by the black box

12–27 August MODIS composite (F -ratio of 78.47 ($P < 0.0001$) in a Welch ANOVA test). The relationship between land cover and $NDVI'$ is strongest in WEB (F -ratio = 64.29, $P < 0.0001$). In ATL, however, $NDVI'$ does not differentiate by land-cover class until well into August (Figure 4), and when tested statistically, it is significant overall (F -ratio = 15.59, $P < 0.0001$), but not strongly different between most land classes.

The clear relationships between $NDVI'$, land cover, and ecological zone confirm that vegetation in the WEB zone was affected earliest and most severely during the 2003 heat wave. On the basis of $NDVI'$ alone, it appears that pastures and cropland within this zone were more seriously affected than forests. Even the relatively modest $NDVI'$ anomaly observed in forests, however, may be indicative of large changes in primary productivity (Ciais *et al.*, 2005), and could have long-term ecological consequences.

3.2. Surface temperature

Maps of the 2003 anomaly in MODIS-derived T_R – calculated in the same manner as the $NDVI$ anomaly – show a springtime maximum in ATL followed by an intense summer maximum that spreads out of WEB in central France (Figure 6). The distribution and timing of the MODIS-detected heat wave is similar to that calculated from meteorological stations and the NCEP/NCAR reanalysis (Figure 7). Averaged over France, all three records report an unseasonably warm April, followed by more typical temperatures in May, a prolonged period of heat in June, and two sharp spikes in the temperature anomaly in July and

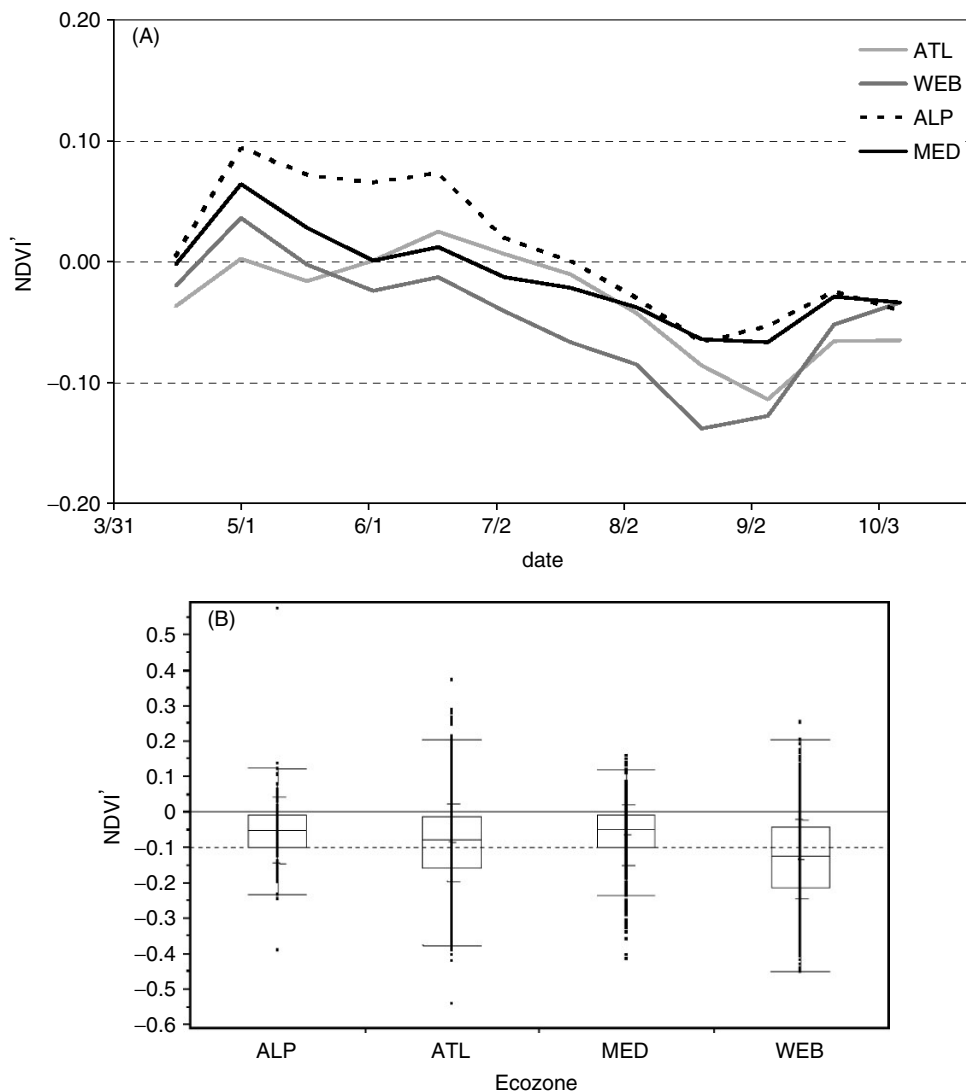


Figure 3. The 2003 anomaly in 16-day MODIS $NDVI$ ($NDVI'$), averaged for each ecological zone. (A) Time series of $NDVI'$ calculated from all pixels, plotted at the mid-date of each composite period. (B) Box plots showing $NDVI'$ for a subsample of pixels in 13–29 August composite period. Boxes contain the 25 and 75% quantiles, and whiskers show the 10 and 90% quantiles. Shorter hatches are the ecozone mean and \pm one standard deviation. The dotted line below the x -axis is the $NDVI'$ mean for the entire study area. Subsampling for the box plots was done through an equally spaced, 10-km grid across the study area ($n = 145, 2302, 491$ and 1816 in ALP, ATL, MED and WEB, respectively)

August. This first-order similarity to conventional temperature records points to the utility of MODIS as a tool for climate monitoring.

As was true for the 2003 $NDVI$ anomaly, ecological zone and land-cover type were significant factors ($P < 0.001$) in explaining spatial variability in the late-season T_R anomaly. This was true whether or not elevation was included as a covariate and whether land-cover type was treated as an independent variable or was nested within the ecological zone designation. The springtime warm anomaly was greatest in ATL and WEB ecological zones, while the June anomaly was significant in WEB and MED. The July and August anomaly peaks were significant and broadly coincident in all three zones, but both were greatest in WEB, where the area-averaged anomaly peaked at 15.6°C in the second week of August (Figure 8). The evolution of

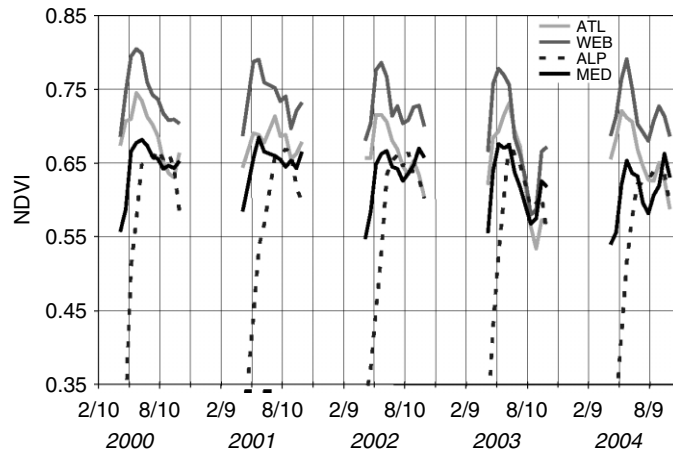


Figure 4. Spring and summer MODIS *NDVI* time series by ecological zone in France, 2000–2004. Data plotted at *NDVI* composite mid-date. Interpolations between missing/corrupted data points in May and July, 2001 are marked by bars along the *x*-axis

the 2003 T_R anomaly varied significantly by CORINE land-cover type within all ecological zones. Averaged across ATL, WEB, and MED, the positive late-summer T_R anomaly was greatest in pastures (Figure 9). Nonirrigated cropland showed a positive spring anomaly, a response to early season drying of the soil in the absence of a full crop canopy, and the positive anomaly for cropland was also large in July and August. Deciduous forests exhibited a moderate anomaly throughout the year. Coniferous forests showed a warm anomaly relative to other land-cover classes in May, when the heat wave was at a minimum, and a cool anomaly relative to other classes in July and August, during the heat wave maximum. This indicates that T_R -detected heat wave was less severe for coniferous forests, owing in part to their setting on north-facing slopes and at higher altitudes (Table II).

It should be noted that T_R derived from MODIS composites represents an average for clear-sky days over the composite period; as clear days tend to be warmer than cloudy days, this may be an overestimate of the actual average T_R . According to the NCEP/NCAR reanalysis, the summer of 2003 was considerably less cloudy than other years in the MODIS record for the study area. This suggests that the potential for warm bias in the composite-based T_R is less in 2003 than in other years, possibly introducing a conservative error to the calculation of radiometric temperature enhancement during the heat wave.

3.3. High-resolution analysis

Although MODIS did capture the spatial variability in heat wave effects, the resolution of the images was poor compared to the scale of land-cover patterns in France. The ASTER sensor offers much higher resolution (15 m shortwave, 90 m thermal) over a smaller image area, providing a clearer look at land use contrasts during the heat wave. A collocated pair of ASTER images from 1 August 2000 and 10 August 2003 show the impacts of the 2003 heat wave on vegetation and surface temperature quite dramatically (Figure 10). Forested areas showed no difference in ASTER-derived *NDVI* between the 2000 and 2003 images (Table III). For pastures and active agriculture, however, *NDVI* dropped by 0.35, or nearly 50%. This result is more dramatic than that obtained from MODIS for the same time period, in large part because mixed pixels in MODIS blur the distinction between land-cover types. Even at ASTER resolution, mixed pixels may cause one to underestimate the difference between land-cover types – when one samples only the interior pixels of pastures and fields one finds an even larger *NDVI* change in 2003, suggesting that hedgerows surrounding agricultural plots are less affected than the crops and grasses themselves.

The difference in land surface temperature between the 2000 and 2003 images is +11 °C for forested pixels and +20 °C for areas classified as pastures or active crops in both images. Within the agricultural land use classes, there was an obvious bimodality between pixels containing a hedgerow, which were relatively

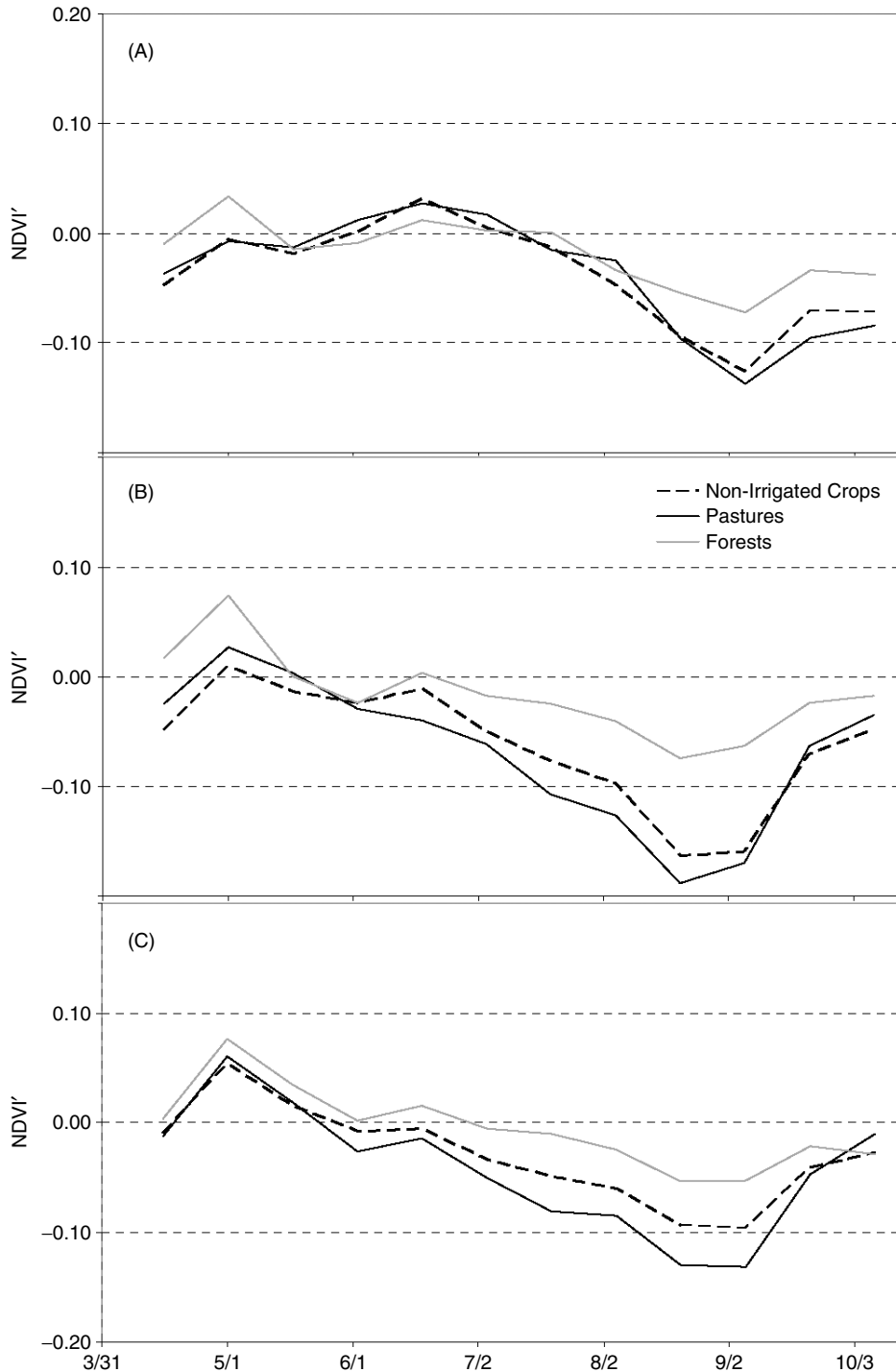


Figure 5. The 2003 MODIS *NDVI* anomaly (*NDVI'*) time series for dominant land-cover types in (A) ATL, (B) WEB, and (C) MED

cool, and hedge-free pixels, which had an average temperature increase of 24 °C. Bare fields were the hottest feature in both images, but fields that were bare in both 2000 and 2003 showed a modest temperature increase (11 °C) relative to active agricultural land. Built-up areas (villages) were also hot in both images but

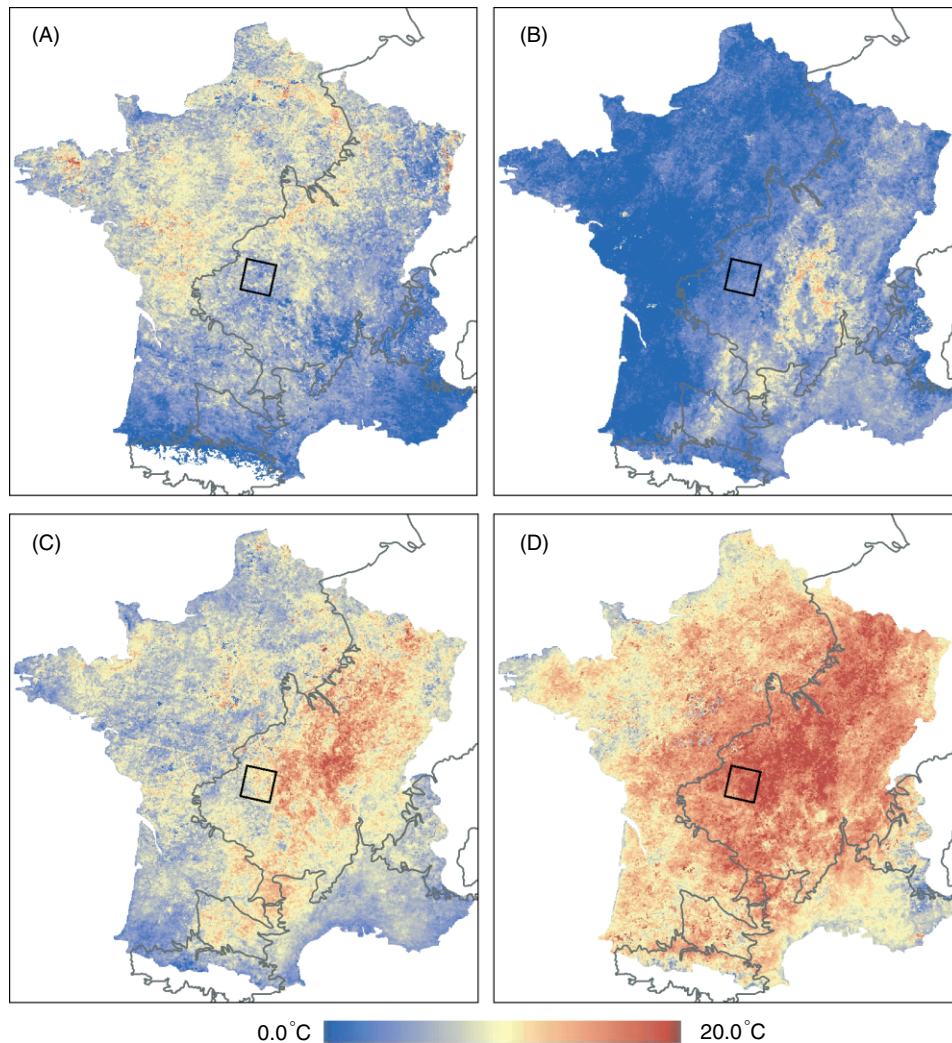


Figure 6. Spatial evolution of the 2003 radiometric temperature anomaly based on 8-day MODIS composites for (A) 15–22 April (B) 10–17 June (C) 12–19 July (D) 5–12 August. Ecological zones are outlined in gray; the ASTER footprint is indicated by the black box

showed the smallest anomaly in surface temperature, at 6°C. The ASTER analysis then confirms that crop and pasturelands experienced a greater increase in T_R than forested areas and further indicates that hedgerows within agricultural lands draw down the average anomaly when viewed at slightly lower resolution.

4. SURFACE ENERGY BUDGET

Many hypotheses regarding the local contribution to climate variability relate to changes in the availability and partitioning of energy at the land surface. For this reason, it is useful to have an accounting of the surface radiation and energy balances before one proceeds to the analyses of local forcings during the 2003 heat wave. The radiation balance as applied here defines net radiation available at the surface (R_{net}) as the sum of incoming and outgoing radiation fluxes:

$$R_{\text{net}} = (1 - \alpha) \times S + \varepsilon_s \times (L_a - L_s) \quad (1)$$

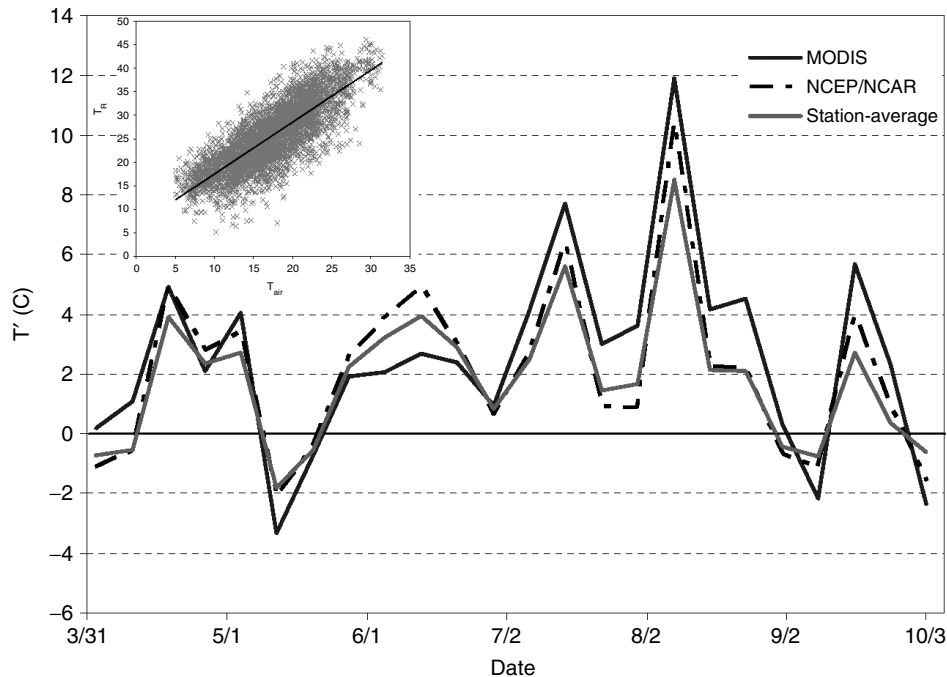


Figure 7. The 2003 temperature anomaly, plotted as 8-day averages for all of France from MODIS (T_R), from the NCEP/NCAR reanalysis ($T_{air}\sigma = 0.995$) and from the average of 126 meteorological stations (T_{air} at 2 m). Inset: Regression of 8-day average 2-m temperature versus MODIS 8-day radiometric surface temperature at the pixel containing the station. Data include all 8-day periods in 2000–2003 for which the mean temperature exceeded 5 °C. The linear fit is $T_R = 1.105T_{air} + 6.4947$, $R^2 = 0.65$

where α is the surface albedo, S is incoming shortwave radiation, ε_s is surface emissivity, L_a is total downwelling longwave radiation at the surface, and L_s is longwave emission from the surface (Table IV, Figure 11). R_{net} is applied to the surface energy balance as

$$R_{net} - G = \lambda E + H = Q_t \quad (2)$$

where G is heat flux into the soil, λE is the latent heat flux, H is sensible heat flux to the atmosphere, and Q_t is the total turbulent energy flux transferred to the PBL (Campbell and Norman, 1998).

4.1. Observations from 2003

Estimates of relevant radiation and energy flux terms are presented in Table V. G was calculated as a function of MODIS-derived T_R , α , and $NDVI$ using an empirical relationship (Bastiaanssen *et al.*, 1998a). Estimates of R_{net} used incoming shortwave radiation from the NCEP/NCAR reanalysis. All values are reported in $W m^{-2}$ and represent mean daily values. In the case of L_s , one estimates the daily mean as the average L_s calculated from the 10 a.m. and 10 p.m. MODIS T_R composites. This approximation is generally accurate within a few degrees, though comparison with available hourly data indicated that the 10 a.m.–10 p.m. proxy was a slight underestimate for daily mean temperature during summer (not shown).

The average white-sky surface albedo derived from MODIS was greatest for ATL throughout the period of analysis (0.18), intermediate in WEB (0.17), and lowest in MED (0.15). Neither the spatial pattern nor the absolute magnitude of albedo changed in 2003 relative to the MODIS era mean. This is somewhat surprising, given the expectation that drought will increase surface albedo (e.g. Eltahir, 1998), but is consistent with some field studies (e.g. Small and Kurc, 2003) and with the ASTER results in the present study (Table III). In the ASTER analysis, the negligible change in broadband albedo can be explained in part by a decrease in near

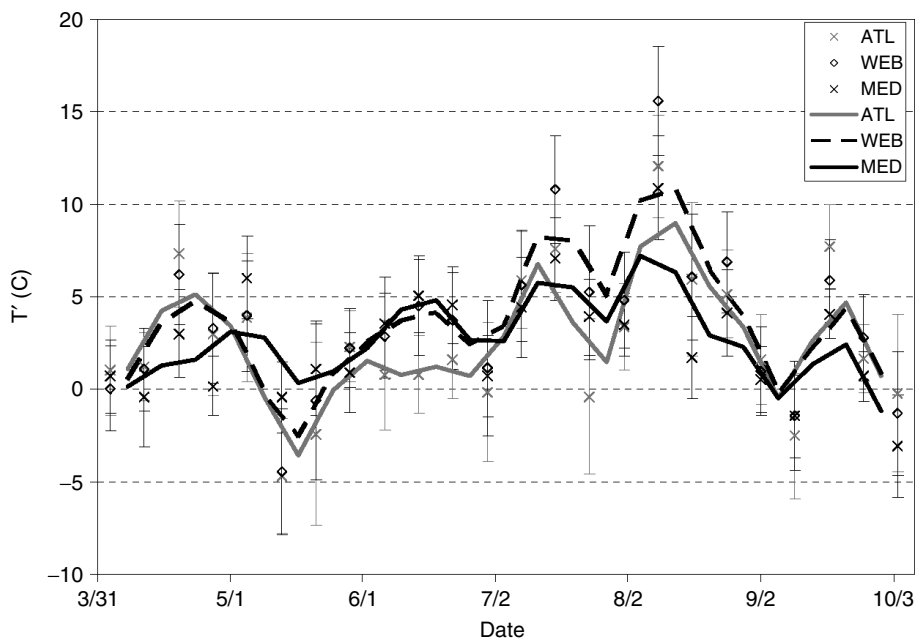


Figure 8. 2003 Radiometric temperature anomaly in each of the three dominant ecological zones. Points indicate the average value for each 8-day composite MODIS image in each ecological zone, error bars indicate \pm one standard deviation within each ecological zone and lines are the 2-point running mean

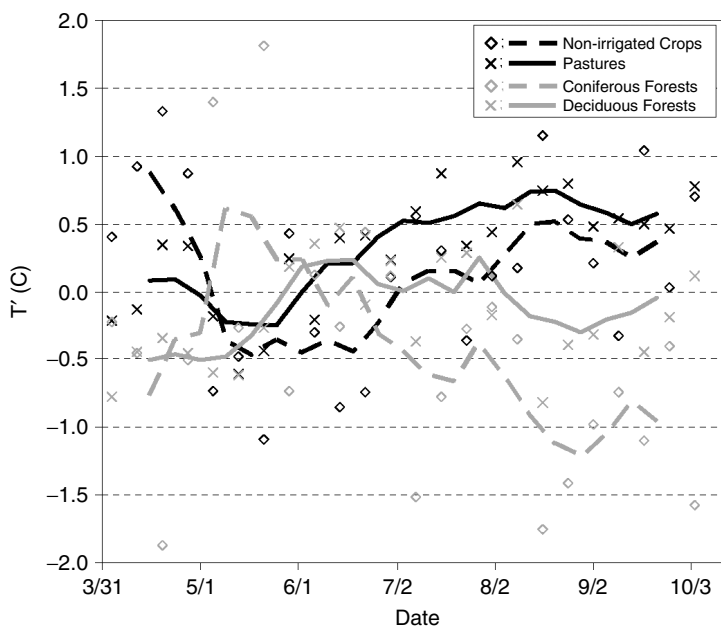


Figure 9. The influence of land cover on MODIS temperature anomaly. Points indicate the 2003 anomaly for each land use calculated relative to the mean 2003 anomaly for France at that date. Lines are the 4-point running mean for 8-day MODIS composite images

infrared reflectivity that offset the increase in reflectivity in the visible range. According to the reanalysis data, there was a substantial increase in incoming shortwave radiation (S) at the surface. This increase was most

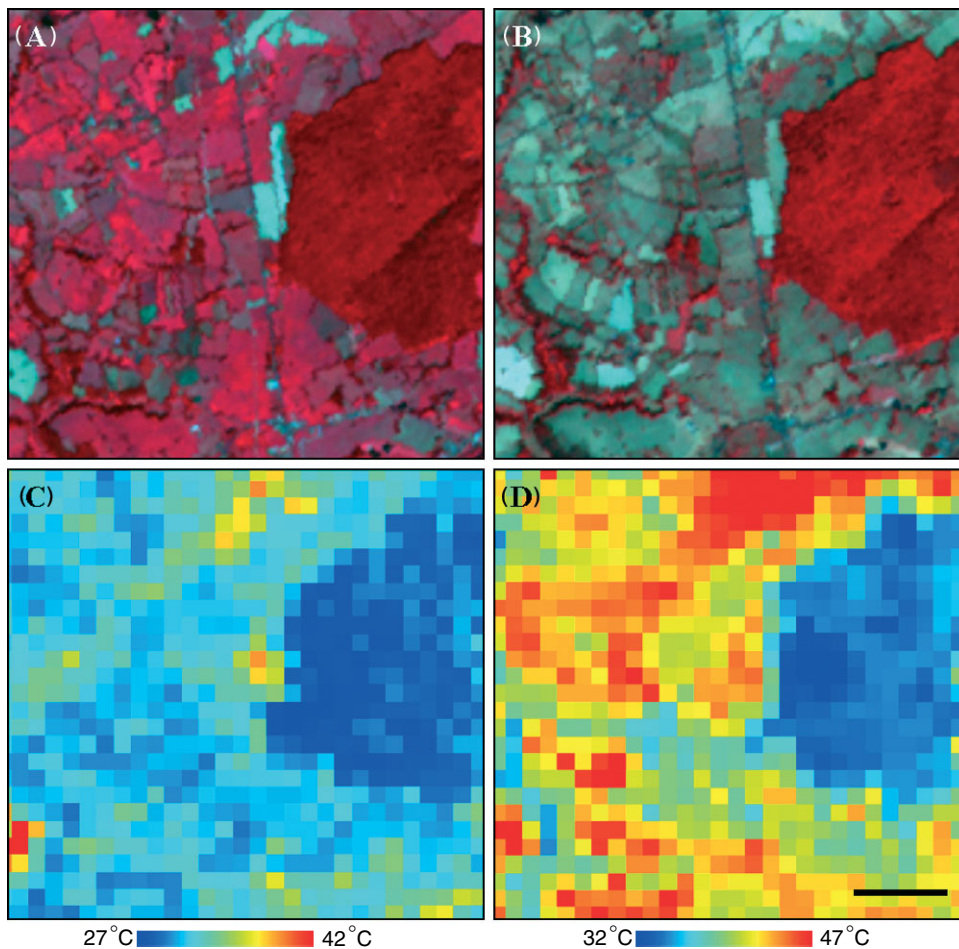


Figure 10. Level 2 ASTER products for a subset of the image footprint. (A), (B) Atmospherically corrected surface reflectances displayed as 321-RGB false color composites for the (A) 1 August, 2000 and (B) 10 August, 2003 images. Vegetation appears red because of the high reflectance in the near-IR (ASTER band 3). (C), (D) ASTER-derived kinematic surface temperature for the same (C) 2000 and (D) 2003 scenes. Note the large contrast between agricultural lands and forest patches in the 2003 image. Scale bar indicates 500 m and applies to all four images

pronounced in ATL and WEB during the April warm period and was large across France in June, July, and August. Because albedo changed little in any zone, absorbed shortwave radiation followed the same pattern as the incoming flux. Emitted longwave radiation is primarily a function of surface temperature, so L_s was greatest in July–August for all zones in all years. The 2003 increase in L_s was also greatest in July–August, corresponding to the period of greatest temperature anomaly, and was largest in WEB throughout the period of analysis. L_s derived from MODIS composites represents an average for clear-sky days over the composite period. As was noted earlier (Section 3), clear days are generally warmer than cloudy days, so MODIS-derived L_s might be an overestimate of the actual average L_s . This potential bias represents a conservative error in the calculation of the average 2003 increase in L_s , since there were fewer cloudy days in 2003 than in other summers.

Average $\varepsilon_s \times L_a$ was largest in July and August, corresponding with the period of highest air temperatures. Interestingly, the 2003 anomaly in $\varepsilon_s \times L_a$ was positive, even though clouds were fewer and the soil was dry. This positive anomaly is the result of elevated air temperature, which has the effect of increasing L_a .

Average R_{net} was greatest in June in all years and was always largest in MED. The overall 2003 reduction in R_{net} , however, was largest in WEB, led by negative anomalies in April and in July–August. MED shared the

Table III. Values of remotely sensed variables and air temperature for the ASTER image pair, 1 August 2000 and 10 August 2003. Bracketed values indicate MODIS averages over the area of the ASTER scene. MODIS $NDVI$ and T_R are derived from single day images and MODIS albedo values are taken from 16-day white-sky albedo composites that include the dates of the ASTER images

Land Cover	Variable	2000	2003	Change
Scene average	T_{air} (°C)	24	32	+8
	$NDVI$	0.73 [0.73]	0.55 [0.50]	-0.18 [-0.23]
	Albedo	0.21 [0.18]	0.20 [0.19]	-0.01 [+0.01]
Forest	T_R (°C)	32 [31]	47 [44]	+15 [+13]
	$NDVI$	0.87	0.87	0
	Albedo	0.19	0.17	-0.02
Villages	T_R (°C)	29	40	+11
	$NDVI$	0.45	0.46	+0.01
	Albedo	0.16	0.15	-0.01
Barren – barren cropland	T_R (°C)	44	50	+6
	$NDVI$	0.27	0.29	+0.02
	Albedo	0.24	0.22	-0.02
Active crops and pastures	T_R (°C)	47	58	+11
	$NDVI$	0.81	0.46	-0.35
	Albedo	0.21	0.22	+0.01
Active crops and pastures (no hedgerows)	T_R (°C)	31	51	+20
	$NDVI$	0.81	0.43	-0.37
	Albedo	0.22	0.22	0
	T_R (°C)	30	54	+24

Table IV. Symbols used in surface energy balance equations and in Table V

Symbol	Definition	Units
α	Albedo	–
ε_s	Surface thermal emissivity	–
ε_{PBL}	Thermal emissivity of the PBL	–
σ	Stefan–Boltzmann constant	$W\ m^{-2}\ K^{-4}$
Bo	Bowen ratio (Bo = $H/\lambda E$)	–
λE	Latent heat flux	$W\ m^{-2}$
G	Heat flux into the soil	$W\ m^{-2}$
H	Sensible heat flux	$W\ m^{-2}$
L	Longwave radiation	$W\ m^{-2}$
L_s	L emitted from the surface	$W\ m^{-2}$
L_a	Total downwards L at surface (NCEP)	$W\ m^{-2}$
L_{PBL}	Downwards L from the PBL	$W\ m^{-2}$
L_{TOA}	Outgoing L at top of atmosphere	$W\ m^{-2}$
Q_t	Turbulent heat flux ($H + \lambda E$)	$W\ m^{-2}$
Q_R	Net radiative heat flux	$W\ m^{-2}$
Q_{Total}	Total heat flux ($Q_t + Q_R$)	$W\ m^{-2}$
R_{net}	Net radiation at the surface	$W\ m^{-2}$
S	Shortwave radiation	$W\ m^{-2}$
T_R	Radiometric temperature	°C
T_{air}	Air temperature	°C
ΔT	Difference between T_R and T_{air}	°C

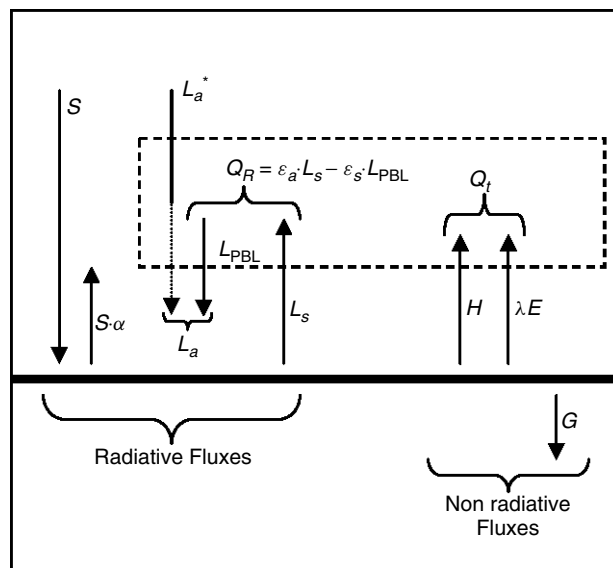


Figure 11. Radiative and nonradiative energy fluxes at the surface. The PBL (dashed box) is assumed to be transparent to shortwave radiation. Terms are as defined in Table IV, with the addition of downwelling atmospheric longwave radiation at the top of the PBL (L_a^*), which is included to show the multiple sources of L_a . The L_a^* vector is dotted to indicate modification by absorption in the PBL

April anomaly but had near-average R_{net} in July–August relative to other years. In ATL there were negative R_{net} anomalies in April and July–August, but both were small relative to a positive anomaly in June, a month in which warm, clear skies made for large incoming fluxes that overwhelmed the increase in L_s associated with soil warming. There is considerable uncertainty in the calculation of G , but the change in 2003 appears to be small relative to other fluxes. All told, the radiation and energy balances yield a decrease in Q_t in all zones in April and July–August and an increase in ATL in June. The decrease was most severe in MED for April (-13.0 W m^{-2}) and in WEB for July–August (-16.1 W m^{-2}). Effects on R_{net} and Q_t were greatest in the daytime, when S was non-zero and L_s was large.

5. SURFACE FORCING ON AIR TEMPERATURE

The land surface is not merely a passive recipient of heat wave and drought. Changes in surface moisture and energy status that occur during a severe drought can lead to anomalous land–atmosphere forcings that enhance near-surface air temperature, influence boundary layer structure, and even alter mesoscale circulations (Chagnon, 1968; Hayden, 1998). The nature of these enhanced forcings varies considerably between regions and land-cover types (Pielke *et al.*, 1991; Pielke, 2001). In this section, two elements of land–atmosphere energy transfer – enhanced sensible heat flux and enhanced emission of longwave radiation – are explored, both of which can act as a local forcing to intensify and prolong heat wave conditions.

5.1. Sensible heat flux

Although satellite-derived temperature estimates generally correlate with near-surface air temperature (Figure 7), there are important and systematic second-order differences between the temperature anomaly calculated from MODIS T_R and the anomaly reported in both station records, which report air temperature at 2 m height, and the NCEP/NCAR reanalysis $\sigma = 0.995$ temperature field, which is an estimate of air temperature at approximately 40 m height. All three records agree on the timing of anomalous warm events, but they disagree on the relative magnitudes of the anomalies: the MODIS T_R anomaly is small relative to

Table V. Major components of the surface energy balance for each ecological zone. Symbols are defined in Table IV. Values are shown for the MODIS era baseline (average from 2000, 2001, 2002, and 2004), for 2003, and for the 2003 anomaly over time periods that correspond to heat wave maxima in April (Julian dates 97–128), June (JD 129–160), July–August (JD 193–224, highlighted in bold type), and the entire period of analysis (JD 97–288)

		Mediterranean			Western European Broadleaf			Temperate Atlantic		
		Mean	2003	Anomaly	Mean	2003	Anomaly	Mean	2003	Anomaly
S	April	265.8	254.8	−10.9	262.3	265.9	3.6	253.5	257.4	3.9
	June	335.5	351.6	16.1	339.7	353.1	13.4	315.1	329.8	14.7
	J-A	287.6	302.9	15.3	285.1	301.2	16.1	267.0	282.9	15.9
	All	279.3	281.9	2.6	279.8	285.9	6.0	264.0	270.4	6.4
$S(1 - \alpha)$	April	227.1	217.3	−9.8	218.9	219.8	0.9	209.0	210.1	1.1
	June	284.0	296.0	12.0	278.6	288.7	10.1	257.1	268.3	11.2
	J-A	261.6	274.7	13.1	253.5	267.9	14.4	238.1	250.4	12.2
	All	237.9	238.8	1.0	231.9	235.7	3.8	217.0	221.1	4.1
L_s	April	369.5	379.6	10.1	359.5	374.8	15.4	362.3	376.4	14.1
	June	423.4	441.2	17.8	406.3	424.2	17.9	405.1	416.1	11.0
	J-A	425.1	455.2	30.2	406.1	447.3	41.2	409.2	436.9	27.7
	All	396.0	407.4	11.5	390.4	405.2	14.7	383.8	394.3	10.5
$L_a \times \varepsilon_s$	April	281.1	287.9	6.8	262.8	268.2	5.4	270.3	278.1	7.9
	June	319.4	329.1	9.6	303.6	315.8	12.2	311.5	323.2	11.6
	J-A	329.4	344.5	15.1	312.0	329.3	17.3	319.5	332.6	13.1
	All	313.5	322.0	8.5	293.2	301.5	8.4	302.2	309.1	6.9
R_{net}	April	138.7	125.7	−13.0	122.2	113.1	−9.1	117.0	111.9	−5.1
	June	180.1	183.9	3.8	175.9	180.3	4.3	163.5	175.4	11.8
	J-A	165.9	163.9	−2.0	159.4	150.0	−9.4	148.4	146.1	−2.3
	All	155.4	153.4	−2.0	134.7	132.0	−2.6	135.4	135.9	0.5
G	April	10.8	10.8	0.0	7.3	8.4	1.1	7.7	9.6	1.9
	June	19.8	22.9	3.1	14.9	18.5	3.7	15.5	17.4	1.9
	J-A	19.0	23.9	4.9	13.9	20.6	6.7	14.8	18.8	4.0
	All	15.3	17.0	1.7	10.3	13.1	2.7	11.8	13.8	2.0
Q_t	April	127.9	114.9	−13.0	114.9	104.8	−10.2	109.3	102.3	−7.0
	June	160.3	161.0	0.7	161.1	161.7	0.7	148.0	157.9	9.9
	J-A	146.9	140.0	−6.9	145.5	129.3	−16.1	133.6	127.3	−6.3
	All	140.1	136.4	−3.7	124.3	119.0	−5.4	123.6	122.1	−1.5
Q_R	April	9.1	8.9	−0.2	8.0	9.0	1.0	4.9	6.0	1.1
	June	12.0	12.4	0.4	8.5	9.7	1.2	7.8	6.0	−1.8
	J-A	9.8	15.0	5.1	5.8	16.6	10.8	6.0	11.7	5.7
	All	4.3	4.4	0.2	7.5	9.3	1.8	0.3	1.0	0.6
Q_{Total}	April	137.0	123.8	−13.2	123.0	113.8	−9.2	114.2	108.3	−5.9
	June	172.2	173.4	1.1	169.6	171.5	1.9	155.8	163.9	8.1
	J-A	156.8	155.0	−1.8	151.3	145.9	−5.3	139.6	139.1	−0.5
	All	144.4	140.8	−3.6	131.8	128.3	−3.5	123.9	123.1	−0.9
L_{TOA}	April	239.7	246.0	6.3	226.9	236.5	9.6	231.5	234.4	2.8
	June	278.1	287.1	8.9	262.5	271.0	8.6	259.0	267.6	8.6
	J-A	278.7	287.4	8.7	260.7	275.2	14.6	256.8	272.0	15.3
	All	264.2	268.0	3.8	249.6	255.1	5.5	250.0	253.8	3.9

the other records in June but larger in July and August (Figure 7). A warm anomaly in September, which occurred after the record-setting heat wave, is also largest in the MODIS estimate.

For the early summer portion of the heat wave, then, the air temperature anomaly exceeded that of T_R , while in late summer the opposite was the case. This implies that the difference between radiometric surface temperature and measured air temperature, $\Delta T = T_R - T_{air}$, was smaller than usual in June and larger

than usual in July and August. Some portion of this pattern can be attributed to the general relationship between T_R and T_{air} , which indicates that ΔT will increase with increasing air temperature (Figure 7, inset). This trend towards increasing ΔT at high temperatures is in part an artifact of comparing two measurements – radiometric and air temperature – that have different physical meanings and sensitivities (Norman *et al.*, 1995; Diak *et al.*, 2004; Mahrt and Vickers, 2004), and also in part due to the fact that on hot, clear days the near-surface temperature gradient is large because of the intense heating of the land surface. It is difficult to separate measurement effects from physical effects, but in either case the influence of the correlation slope is only 0.1°C per degree increase in air temperature. This correlation slope cannot explain the bulk of the variability observed in ΔT . In early August, for example, the average air temperature anomaly reported at French meteorological stations reached 8.5°C . The $T_R - T_{air}$ offset explained by the regression, then, would be 0.85°C . In this study, the observed offset for this period was 3.4°C . Furthermore, the 2003 T_R anomaly exceeded the T_{air} anomaly in both April and September but not in June, even though air temperature was higher in June. These results suggest that temporal variability in ΔT is primarily driven by changes in surface and weather conditions and not by a general tendency to increase with increasing air temperature.

Variability in ΔT is of interest because the difference between surface and air temperature can be related to sensible heat flux (H), approximately as

$$H = c_p \rho_{air} \beta \times \Delta T \times u \times C_{ah} \quad (3)$$

where c_p and ρ_{air} are the specific heat and density of air, C_{ah} is an adjusted aerodynamic conductance, u is windspeed, and β is a parameter that adjusts for differences between the radiometric temperature, as measured by satellite, and the surface aerodynamic temperature relevant for heat flux calculations ($0 < \beta < 1$) (Chehbouni *et al.*, 1997).

Determining appropriate values for C_{ah} and β is not trivial. Here an attempt is made to minimize the influence of these parameters by calculating the 2003 sensible heat flux as a % change ($H_{\%}$) from the average value at that location for each composite period: $H_{\%}(x, y, P) = 100 \times H_{2003}(x, y, P) / \overline{H}(x, y, P) - 100$, where \overline{H} is the MODIS era baseline at pixel location (x, y) for composite period (P) , with P defined as the 8-day Julian Date range of a MODIS composite image. In this framework, the sensible heat relationship is simplified as follows:

The aerodynamic conductance, C_{ah} (m s^{-1}), is conventionally defined as

$$C_{ah} = \frac{k^2}{\ln\left(\frac{z_m - d}{z_{0m}} - \Psi_m\right) \times \ln\left(\frac{z_h - d}{z_{0h}} - \Psi_h\right)} \quad (4)$$

where z_{0m} and z_{0h} are the roughness lengths for momentum and heat, respectively (m), z_m and z_h are the heights at which wind and humidity are recorded, d is the displacement height (m), k is von Karman's constant (0.41), and Ψ_m and Ψ_h are parameters of atmospheric stability, set to zero for neutral conditions (Choudhury *et al.*, 1986). Following the Businger–Dyer formulation of roughness length for heat transfer, the terms $(z_m - d)/z_{0m}$ and $(z_h - d)/z_{0h}$ can be set to constants for a common land use at a common solar elevation angle (Sugita and Brutsaert, 1990). Changes in vegetation health can undermine this assumption, but the influence on roughness of crop and grass vigor is minimal in a hedgerow landscape and for closed forests (Lagouarde *et al.*, 2002; Hasager *et al.*, 2003). Additionally, the terms Ψ_m and Ψ_h are not particularly sensitive to moderate instability. This yields C_{ah} approximately constant for common land cover, date, and stability conditions.

Variability in the term for radiometric adjustment, β , is also minimized when one controls for seasonal and spatial heterogeneity. There is evidence, however, that β is a function of vegetation health, with values converging at 1.0 for a full, healthy canopy, and dropping below 1.0 for sparse canopies and stressed vegetation (Chehbouni *et al.*, 1996). This is an obvious complication in the study of drought, as the failure to account for interannual changes in β could cause one to overestimate the sensible heat flux anomaly associated with the 2003 heat wave. Rather than attempt to estimate β over all pixels in every MODIS image, one controls for the

parameter indirectly by calculating two separate estimates of $H_{\%}$. First one calculates $H_{\%}$ for pixels classified as pasture and makes no adjustment for β . This represents a high-end estimate, as pastures had relatively large anomalies in T_R and $NDVI$, and it is possible that β or C_{ah} decreased during the drought. Next one calculates $H_{\%}$ for forested pixels in which the $NDVI$ anomaly never dropped below -0.1 . These areas had a full canopy throughout the heat wave – so β in 2003 should be relatively similar to β in other years – and the impact of the heat wave was modest both in terms of $NDVI'$ and the T_R anomaly. Pixels of this type thus represent a 'conservative' estimate of $H_{\%}$ and an indirect control on β effects. For the results presented here, NCEP/NCAR reanalysis data for $\sigma = 0.995$ have been used to provide wind and air temperature data at a near-surface blending height. The calculation was repeated in subset regions using wind speed and air temperature interpolated from meteorological station records. Results were similar, and are not shown.

Figure 12 shows the evolution of $H_{\%}$ from April to October, plotted as a range between the high-end and the conservative estimates described above. By this measure, the sensible heat flux anomaly in MED was modest and relatively constant throughout spring and summer. This is consistent with expectation, as summertime dessication is a regular phenomenon in MED, and the dry land surface of the region probably acted as a substantial local heating source in all years of the MODIS record. The present results are also consistent with sensible heat flux measurements recorded at the EUROFLUX station at Puechebon, located in a mixed broadleaf and evergreen forest within MED (Figure 1). The $H_{\%}$ for Puechebon, calculated using the average clear-day sensible heat flux for each 8-day compositing period, shows no significant seasonal trend, with values averaging $\pm 15\%$ for the entire period of analysis (Figure 12).

In WEB $H_{\%}$ has a greater temporal structure. There is a brief positive anomaly in April, associated with the warm, dry spring, followed by a prolonged period of below-average sensible heat flux that lasts through the month of June. This suggests that the high air temperatures in June were a product of large-scale synoptic processes with relatively small contribution from local surface heating. Over the course of July, however, $H_{\%}$ climbs dramatically, peaking at 48–61% in August. In late August and September, $H_{\%}$ gradually returns to more typical values, though the anomaly persists at about 20% into October. The sensible heat flux anomaly measured at the EUROFLUX site in Hesse experimental forest, a broadleaf deciduous forest located within WEB, follows the same general pattern as MODIS-derived $H_{\%}$. In late August and September, however,

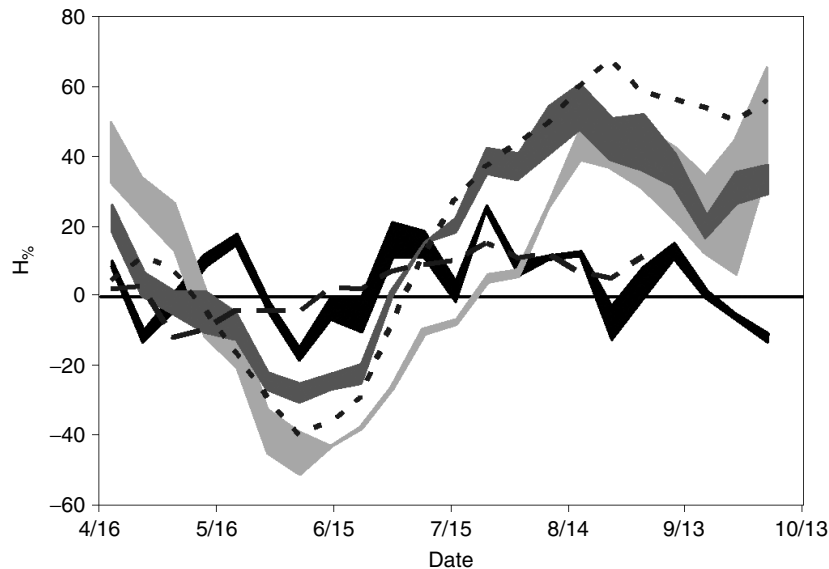


Figure 12. 2003 sensible heat flux anomaly, calculated from MODIS and reanalysis data. Shaded time series are the 4-pt running average of 8-day MODIS composites for Mediterranean (dark gray), Western European Broadleaf (medium gray) and southern temperate Atlantic (light gray) ecological zones. Width represents the range between high and low estimates, as described in the text. Dashed line is the 4-pt running average of 8-day mean sensible heat flux measured at the EUROFLUX tower at Puechebon (Mediterranean zone) and dotted line is the same from EUROFLUX Hesse Forest (Western European Broadleaf zone)

the percent change measured at Hesse was larger than the MODIS-derived $H_{\%}$ in the present case, and this was true both for the ecological zone average and for MODIS pixels closest to the EUROFLUX site. The discrepancy could be due to local conditions at the EUROFLUX site or to the failure of one of the assumptions made. If, for example, the increased sensible heat flux of 2003 was associated with a significant destabilization of the PBL at Hesse, then the assumption that C_{ah} was constant would yield a conservative error in the estimate of $H_{\%}$.

The evolution of $H_{\%}$ in ATL is similar to that in WEB, but the springtime maximum is more pronounced, the June minimum is deeper, and the increase to high values in late summer comes later, reaching a value of 37–51% by the middle of August. In September, $H_{\%}$ in ATL actually exceeds that in WEB, especially for pastures and croplands. For all three zones, $H_{\%}$ correlates primarily with the anomaly in ΔT , with anomalies in u playing a secondary role. Given an average summertime sensible heat flux of 50 W m^{-2} in ATL and WEB (Räisänen *et al.*, 2004), the 37–51% enhancement for August in ATL corresponds to a $18.5\text{--}25.5 \text{ W m}^{-2}$ increase in sensible heating and the 48–61% enhancement in WEB corresponds to a $24.0\text{--}30.5 \text{ W m}^{-2}$ increase. The June minima of -25 to -30% in WEB and -40 to -50% in ATL, meanwhile, would correspond to $12.5\text{--}15.0 \text{ W m}^{-2}$ and $20.0\text{--}25.0 \text{ W m}^{-2}$ decreases in sensible heating, respectively.

5.2. High-resolution analysis

To further examine the influence of land-cover type on sensible heat flux, one again turns to the ASTER image pair. For these high-resolution, small area images, one has greater confidence in one's ability to parameterize a full model for sensible heat flux. The surface energy balance algorithms for land (SEBAL) model (Bastiaanssen *et al.*, 1998a), has been applied with success in a number geographical contexts (Bastiaanssen *et al.*, 1998b) including southern France (Lagouarde *et al.*, 2002). SEBAL involves a series of calculations through which satellite images are combined with basic meteorological station data to calculate spatially distributed sensible and latent heat flux from the land surface. Sensible heat flux is calculated using the relationship expressed in Equation (3), with iterative correction for the influence of atmospheric stability on the conductance term defined in Equation (4). The model is relatively simple, which facilitates its application across diverse landscapes, but the results are sensitive to the correction applied to radiometric temperature for flux calculations (analogous to the β -problem discussed earlier) and to the determination of C_{ah} for each land-cover type. In this application, one uses the linear correction for radiometric temperature suggested in Bastiaanssen *et al.* (1998a), which defines the near-surface air temperature gradient as a linear function of radiometric surface temperature, $\Delta T = aT_r + b$, where the coefficients a and b are determined by inverting the sensible heat flux equation at 'hot' and 'cold' end member pixels within the satellite image. The linear correction is appropriate for a single satellite image of limited footprint. It must be applied independently for images from different dates, in order to account for variability associated with weather or surface conditions, and for large images it should be applied at multiple locations within the image footprint (Bastiaanssen *et al.*, 1998a). Uncertainty regarding C_{ah} largely derives from the difficulty in estimating roughness lengths for heterogeneous landscapes. Following the work from heterogeneous landscapes in southern France (Jacob *et al.*, 2002) and Denmark (Hasager *et al.*, 2003), a neutral-stability C_{ah} of 0.10 m s^{-1} was estimated for forest patches and 0.04 m s^{-1} for the agricultural matrix of pastures, croplands, and hedgerows. Reference meteorological data were obtained from the average of three meteorological stations located in the vicinity of the ASTER image.

Averaged over the ASTER image, SEBAL estimates for instantaneous (10 a.m.) sensible heat flux are $227.7 (\pm 119.3) \text{ W m}^{-2}$ and $134.5 (\pm 86.8) \text{ W m}^{-2}$ for forests and the agricultural matrix (excluding bare soil), respectively, in 2000. The \pm here represents the one standard deviation variability in ΔT within land-cover class. In 2003, the algorithm yields $281.6 (\pm 128.8) \text{ W m}^{-2}$ for forests and $335.4 (\pm 82.4) \text{ W m}^{-2}$ for agriculture. The sensible heat flux for bare soil was not calculated because of the difficulty of estimating near-surface stability and temperature-correction terms. Variability within land-cover type is large relative to the difference between forests and agricultural lands, but the calculation indicates that the 2003 enhancement in sensible heat flux was greater for agricultural lands than for forests. This is consistent with expectation,

as the shallow-rooted vegetation typical in pastures and croplands does not have access to deeper reservoirs of water and dries more quickly than deeper-rooted forest canopy vegetation during a drought, leading to a rapid increase in sensible heat flux (e.g. Shukla *et al.*, 1990).

The SEBAL 2000 sensible heat fluxes are similar to those recorded for forests and agricultural fields in the HAPEX–MOBILHY experiment, conducted in the summer of 1986 in southwest France (Noilhan *et al.*, 1991), and the SEBAL flux for forests in both 2000 and 2003 falls in the range of 10 a.m. values recorded at the EUROFLUX sites in Hesse and Puechebon in early August of that year. Relative to MODIS estimates, the SEBAL percentage increase in sensible heat flux is small for forests and large for agricultural lands. This suggests that mixed pixels blurred the distinction between these land-cover types at the scale of MODIS resolution.

It is also worth noting that the *absolute* sensible heat flux from agriculture is estimated to exceed that from forests in the 2003 ASTER scene. If accurate, this is a surprising reversal of the usual landscape pattern of sensible heat flux – in previous studies, forests have been found to have a larger daytime sensible heat flux than agricultural lands, an effect that is attributed to the forest's low albedo and large surface roughness (e.g. Bougeault *et al.*, 1991). The present result suggests that pastures and croplands may have played a dominant role in the local forcing during the 2003 heat wave. The result is, however, sensitive to the parameterization of SEBAL and to transient changes in soil moisture associated with rain events.

5.3. Radiative heating

In addition to the sensible heat flux, the surface warms the atmosphere radiatively through surface longwave emission (L_s). The portion of L_s that is absorbed in the PBL depends on the absorptivity/emissivity of the PBL, ε_{PBL} (Table IV). At the same time, the PBL is emitting longwave radiation at a rate dependant on both ε_{PBL} and air temperature: $L_{\text{PBL}} = \varepsilon_{\text{PBL}} \times \sigma \times T_{\text{air}}^4$, where σ is the Stefan–Boltzmann constant. For the lower atmosphere, then, one can define a net longwave radiative exchange (Q_{R}) that is the difference between L_s absorbed in the boundary layer and L_{PBL} that is absorbed at the surface: $Q_{\text{R}} = (\varepsilon_{\text{PBL}} \times L_s) - (\varepsilon_s \times L_{\text{PBL}})$. As this definition accounts for both emission and absorption of radiation within a well-mixed boundary layer, it can be thought of as an estimate of the effective heating of the lower atmosphere by the surface due to the convergence of longwave flux.

In order to calculate Q_{R} , one estimates ε_{PBL} using a broadband emissivity approach (Liou, 2002). For a typical specific humidity of 10 g kg^{-1} , a CO_2 concentration of 350 ppmv, and an average PBL depth of 1 km, the broadband flux emissivity (ε_{PBL}) is approximately 0.5 for water vapor and 0.17 for CO_2 (Liou, 2002). Because of overlapping absorption spectra, these values are not strictly additive, but 0.6 is a reasonable, conservative estimate for emissivity, and therefore flux absorptivity, in the PBL. Values of ε_s were obtained from MODIS (mod11a2), and tended to be near unity for vegetated surfaces. In order to be consistent with the calculation of sensible heat flux, one uses T_{air} from NCEP/NCAR $\sigma = 0.995$ in the calculation of radiative flux as well.

For the 2003 heat wave, the anomaly in L_s was substantial: averaged over April–September there was a $+12.6 \text{ W m}^{-2}$ anomaly in MODIS-derived L_s for all of France. This anomaly can be attributed entirely to elevated T_{R} , as MODIS-derived surface emissivity did not change detectably in 2003. During the period corresponding to the late-summer peak of the heat wave (Table V, July–August) the L_s anomaly in WEB was $+41.2 \text{ W m}^{-2}$. For $\varepsilon_{\text{PBL}} = 0.6$, this gives an anomaly in radiative heating of the PBL of $+7.6 \text{ W m}^{-2}$ for France over the entire period and area of analysis, and $+24.7 \text{ W m}^{-2}$ for WEB during the July–August heat wave maximum. Elevated air temperatures over those periods would produce anomalies in surface absorption of downwelling radiation from the PBL of $+6.5 \text{ W m}^{-2}$ and $+13.9 \text{ W m}^{-2}$, respectively. This yields an anomaly in net longwave radiative exchange (Q_{R}) of $+1.1 \text{ W m}^{-2}$ for all of France for April–September and $+10.8 \text{ W m}^{-2}$ for WEB for July–August (Table V). During the heat wave maximum, then, the anomaly in net radiative heat flux is on the same order of magnitude as that in sensible heat flux, and it should be included in any calculation of surface heating of the PBL. The ASTER analysis demonstrates that the L_s anomaly was greatest in crops and pastures; so, as was the case for sensible heat flux, those land-cover types would have contributed most strongly to the radiative heating of the PBL.

The preceding analysis accounts only for clear-sky emissivity in the PBL. It has been observed, however, that total atmospheric cloudiness was reduced in 2003 relative to other years (e.g. Black *et al.*, 2004), a fact that contributed to the enhanced outgoing longwave radiation at the top of the atmosphere during the heat wave (L_{TOA} , Table V). As clouds above the boundary layer can reradiate absorbed longwave radiation back into the PBL, reduced cloud emission in 2003 could have compensated for enhanced surface-to-PBL heating during the heat wave. The fact that the total downwelling longwave radiation flux at the surface reported in the NCEP/NCAR reanalysis (L_a , Table V) had a positive anomaly throughout the heat wave, however, suggests that reduced downward emission from clouds was a secondary effect in the radiation budget of the lower atmosphere.

6. POTENTIAL FOR PRECIPITATION FEEDBACKS

The intensity and spatial structure of the 2003 heat wave described above provide observational evidence for a surface forcing on temperature that was strongest in the WEB ecological zone. The summer of 2003 was also characterized by significantly below-average precipitation, but in this case it is not obvious whether the precipitation anomaly was entirely a product of the large-scale circulation or whether the land surface also played a role. Nevertheless, models suggest that a soil-moisture precipitation feedback will become important in the future climate of Europe (Schär and Jendritzky, 2004; Vidale *et al.*, 2005). In this section, the consistency of the surface energy balance and drought measurements are evaluated with a number of different mechanisms proposed for potential soil-moisture precipitation feedbacks generally, and for soil-moisture feedbacks invoked in models of future European climate in particular.

6.1. Three proposed mechanisms

Several mechanisms have been proposed for a land–atmosphere feedback affecting local precipitation. Perhaps the most intuitive is precipitation recycling, in which water evaporated from the land surface contributes to the local formation of clouds and precipitates in the form of rain (Brubaker *et al.*, 1993; Eltahir and Bras, 1996). Anomalies in soil moisture may influence precipitation rates simply by increasing or decreasing the local flux of water vapor into the lower atmosphere. In most regions, however, only a small fraction of evaporated water is recycled as precipitation near the source area (Trenberth, 1999), and in regions like Western Europe – where the atmospheric water budget is dominated by external vapor flux (Schär *et al.*, 1999) – natural variability in local evaporation has only a small influence on bulk humidity.

A second way in which the land surface may influence local precipitation is through stabilization or destabilization of the PBL (Betts and Ball, 1998). In this mechanism, drying of the soil surface causes an increase in the Bowen ratio (the ratio of sensible heat flux to latent heat flux) that, in turn, leads to a deepening of the daytime PBL with increased entrainment of dry, low-energy air from above the boundary layer. Entrainment and an increased Bowen ratio combine to cause a decrease in the density of water vapor and moist static energy (MSE) within the PBL and reduced potential for convective precipitation. This has been termed the ‘indirect’ soil-moisture precipitation feedback, since it relies upon the concentration and convection of water vapor and does not require that the water vapor be generated locally.

The indirect feedback pathway must be considered in tandem with a third proposed feedback involving R_{net} (Eltahir, 1998). Under drought conditions, when vegetation is stressed and the soil surface is hot and dry, L_s increases and, generally, α increases (though this was not observed in 2003 – see Section 4). This causes a reduction in net radiation (R_{net}) available at the surface (Equation (1)). Assuming a surface energy balance (Equation (2)), reduced R_{net} is associated with a drop in Q_t and a decrease in the local production of MSE. Under drought conditions, the combined processes of reduced local production of MSE (Eltahir, 1998), decreased concentration of MSE in a deepened PBL (Betts and Ball, 1998; Eltahir, 1998), and increased entrainment at the top of the PBL (Betts and Ball, 1998) can exert a negative forcing on precipitation.

In a modeling study of the role played by soil moisture in the European climate, Schär *et al.* (1999) found significant effects of soil moisture on summer precipitation patterns in France. Regional climate

simulations forced with a dry soil surface (DRY) returned less precipitation than simulations forced with either a wet soil surface (WET) or realistic (CTRL) surface conditions. Their model results indicated that surplus precipitation in the WET simulation derived primarily from atmospheric advection, and that the soil-precipitation feedback operated through both proposed 'indirect' pathways: in the DRY simulation, sensible heat flux was enhanced, with an average July Bowen ratio (\mathbf{Bo}) of $\mathbf{Bo} = 9.7$, relative to $\mathbf{Bo} = 0.93$ in the CTRL simulation and $\mathbf{Bo} = 0.44$ in WET, while Q_t in DRY was 17.1 W m^{-2} less than in WET because of an increase in L_s , effecting a decrease in the total MSE in the boundary layer. One wishes to see if either of these modeled feedback processes is consistent with the present observations from the heat wave of 2003.

6.2. Potential for soil-precipitation feedbacks in 2003

Using the estimate that August sensible heat flux in WEB was enhanced by about 25 W m^{-2} relative to the MODIS baseline (Section 4), one obtains a Bowen ratio of $\mathbf{Bo} = 1.92$ for 2003 *versus* $\mathbf{Bo} = 0.72$ in the MODIS-era baseline. These values of \mathbf{Bo} are intermediate relative to the simulations of Schär *et al.* (1999), and they are on the same order as those observed during field studies of soil-precipitation processes (Betts and Ball, 1998). In both models and field observations, such a change in Bowen ratio was associated with a deepening and stabilization of the daytime PBL, suggesting that a similar process may have operated during the heat wave of 2003. It should be noted, however, that the same analysis would suggest a forcing towards precipitation *enhancement* during June of 2003, when \mathbf{Bo} was reduced relative to the MODIS baseline, so the case for a feedback related to stabilization of the PBL is not clear-cut.

Evidence for a precipitation forcing associated with reduced Q_t is also mixed. The magnitude of the calculated 2003 anomaly in Q_t (Section 4) exceeds 10 W m^{-2} in both MED and WEB in April (Table V), and during the July–August maxima, the Q_t anomaly in WEB (-16.1 W m^{-2}) is similar to the mean daily difference between WET and DRY model simulations (-17.1 W m^{-2} ; Schär *et al.*, 1999). During June, however, the Q_t anomaly is near zero in MED and WEB and is strongly positive in ATL. Additionally, the 2003 anomalies in Q_t and net longwave radiative transfer (Q_R ; Section 5) tend to offset one another. At the peak of the heat wave, when the 2003 Q_t anomaly in WEB is -16.1 W m^{-2} , the anomaly in the radiative balance between land surface and the PBL is $+10.8 \text{ W m}^{-2}$. The negative anomaly in total surface heating of the atmosphere (turbulent plus radiative), then, was modest – only -5.3 W m^{-2} – even at the peak of the heat wave (Table V). During June, the anomaly in total surface heating of the lower atmosphere was actually positive, as high as $+8.1$ in ATL, suggesting a potential for a positive forcing on precipitation during a period of developing drought. This result runs counter to the precipitation feedback theory and further emphasizes the distinct character of the June warm period *versus* the July–August heat wave maximum. Only during the springtime warm period was there a strong signal of reduced total energy transfer from the surface, ranging from -5.9 W m^{-2} in ATL to -13.2 W m^{-2} in MED. This springtime result is consistent with a negative forcing on precipitation related to reduced local production of MSE, but it holds only for April.

7. CONCLUSIONS

The spring of 2003 was unusually warm throughout Western Europe. In France, the average 2-m April air temperature was $1.3 \text{ }^\circ\text{C}$ higher than the average for 2000–2002 and 2004 (the 'MODIS era baseline'), with an 8-day average maximum anomaly of $+3.9 \text{ }^\circ\text{C}$ in the third week of the month (Figure 7). This spring warmth led to an early green-up (Figure 5) that was greatest in forested areas of the WEB and MED ecological zones. In agricultural lands there is some evidence that springtime warmth led to a drying of the soil and an early-season enhancement in sensible heat flux (Figure 12), particularly in the Atlantic ecological zone (ATL) in the north of the country. Overall, however, there was a reduction in total energy transfer from the surface to the PBL (Q_{Total}) of 5.9 W m^{-2} in ATL, 9.2 W m^{-2} in the WEB zone (WEB), and 13.2 W m^{-2} in the MED ecological zone. This combination of enhanced sensible heat flux and reduced Q_{Total} is consistent with hypotheses of a soil-moisture precipitation feedback in which drying of the soil leads to a reduced potential for convective precipitation (Betts and Ball, 1998; Eltahir, 1998).

After a respite in late spring, a second positive temperature anomaly developed in June. Average air temperatures exceeded the MODIS era baseline by 3.1°C , with a maximum 8-day anomaly of 5.0°C in MED at the middle of the month (Figure 8). At this time the *NDVI* anomaly was near zero in both MED and ATL – only WEB showed the beginning of a vegetation drought that developed over the course of the month (Figures 3 and 4). In contrast to warm periods in April and in July and August, the calculated anomalies in surface sensible heat flux in June were near zero in MED (Figure 12) and were strongly negative in both WEB (-12.5 to -15.0 W m^{-2}) and ATL (-20.0 to -25.0 W m^{-2}). The anomaly in Q_R , meanwhile, was near zero in all zones (Table V). These results suggest that the June portion of the heat wave was largely an advection phenomenon. Synoptic-scale weather patterns contributing to the development of the early summer heat anomaly have been described in detail elsewhere (Black *et al.*, 2004). In general, the subtropical Azores anticyclone was extended northward in May and June, causing anomalously high pressure and warm advection in Western Europe (Figure 13).

The heat wave abated briefly at the end of June before rising to a maximum in late summer, punctuated by peaks in the 8-day air temperature anomaly in mid-July ($+5.6^{\circ}\text{C}$) and early August ($+8.5^{\circ}\text{C}$). This period corresponded with a significant negative anomaly in *NDVI* throughout France. The negative anomaly developed first in mid-June in WEB (Figures 2 and 3(A)) and later in MED and ATL. By the end of July there was a substantial negative anomaly in all three ecological zones, and by the middle of August the domain-wide anomaly was -0.1 (Figure 3(B)). The anomaly was most severe in WEB and was greatest for pastures and nonirrigated crops in all zones.

It was also in July and August that the surface forcing on air temperature reached its maximum. The 8-day average radiometric temperature anomaly (T_R) approached $+12^{\circ}\text{C}$ across all of France (Figure 7), and the sensible heat flux anomaly reached 48–61% (24.0 – 30.5 W m^{-2}) in WEB and 37–51% (18.5 – 21.5 W m^{-2}) in ATL. These anomalies in sensible heat flux are similar to the 40–80% increase that climate models predict for July and August in France in the late twenty-first century (Räisänen *et al.*, 2004). The sensible heat flux anomaly remained small in MED throughout this period, indicating that the heat wave did not significantly alter the partitioning of surface energy in this drought-prone ecological zone. A positive anomaly in net longwave radiative exchange (Q_R) also contributed to enhanced surface heating of the lower atmosphere. The Q_R anomaly in July–August was $+10.8\text{ W m}^{-2}$ in WEB and $+5.1\text{ W m}^{-2}$ and $+5.7\text{ W m}^{-2}$ in MED and ATL, respectively, reflecting extremely high radiometric surface temperatures in all three zones at this time. ASTER images from WEB in early August indicate that the anomalies in radiometric temperature, sensible heat flux, and Q_R were all greatest in agricultural lands and smallest in forests.

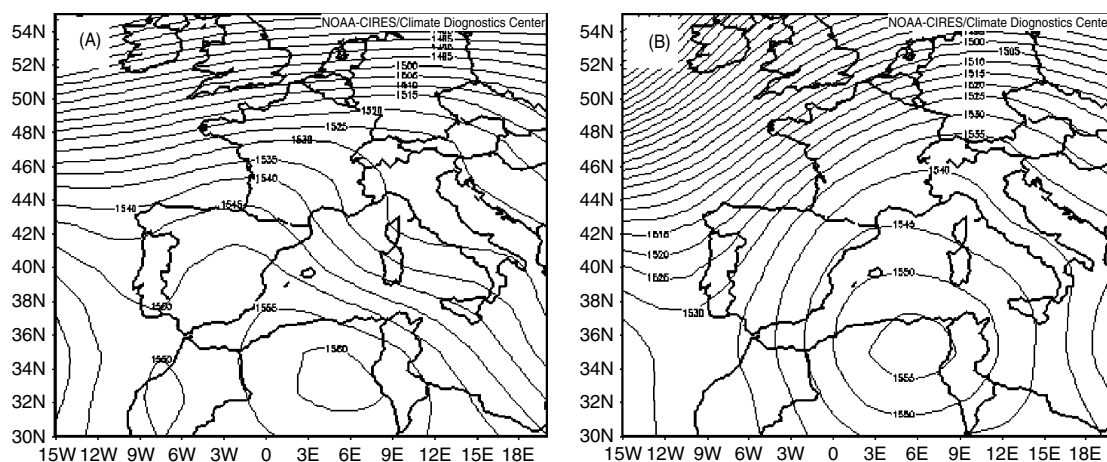


Figure 13. Mean 850-hPa Geopotential Height (m) for June in (A) the MODIS era baseline and (B) 2003, derived from the NCEP/NCAR reanalysis. Image provided by the NOAA-CIRES Climate Diagnostics Center, Boulder Colorado from their Web site at <http://www.cdc.noaa.gov/>

Table VI. Schematic summary of results for the Western European Broadleaf (WEB) ecological zone. Upward arrows indicate a positive anomaly in 2003, downward arrows a negative anomaly, and dashes an anomaly near zero. Size of arrows represents magnitude of anomaly relative to other time periods. Symbols are defined in Table IV

	T_R, T_{air}	$NDVI$	H	Q_t	Q_R	Q_{Total}
April	↑	↑	↑	↓	–	↓
June	↑	–	↓	–	–	–
July–August	↑	↓	↑	↓	↑	↓

The positive anomaly in sensible heat flux in WEB and ATL in July and August was accompanied by a substantial increase in the Bowen ratio. Both of these observations indicate a potential for surface-induced deepening and drying of the PBL, consistent with the Betts and Ball (1998) mechanism for suppression of convective precipitation. Evidence for a precipitation feedback related to the local production of MSE (Eltahir, 1998) was not as strong, as a significant negative anomaly in turbulent energy transfer (Q_t ; Table V) was nearly offset by a positive anomaly in Q_R .

In summary (Table VI), the results of this study indicate that the heat wave of 2003 bore a phenomenological resemblance to model-predicted summers of the late twenty-first century (e.g. Räisänen *et al.*, 2004). There was an unusually early spring green-up in response to the high temperatures in April. This was followed by a severe late-summer drought that was greatest in the ‘transitional belt’ between MED and ATL climate zones. The temperature anomaly was largest in south central France and was associated with substantially enhanced sensible heat flux. These results are consistent with various models of regional climate change, lending independent support to the model-based claim that the heat wave of 2003 was similar to the potential future summertime climate of Europe (Schär *et al.*, 2004). Observations regarding the potential for soil-moisture precipitation feedbacks are less consistent. In spite of these mixed results, the observational approach utilized in this study provides a useful counterpart to numerical models of soil-moisture precipitation feedbacks. In this application, the satellite-based observation of a substantial anomaly in radiative heating from the surface demonstrates that heating by longwave radiation should not be overlooked in studies of feedback processes.

This study further suggests that extreme heat waves have implications for ecology and land management. A number of studies focused on trends in $NDVI$ across the higher latitudes, for example, have documented an *increase* in mean $NDVI$ associated with the warming of recent decades (Zhou *et al.*, 2001; Zhou *et al.*, 2003; Stöckli and Vidale, 2004). For Europe specifically, Stöckli and Vidale (2004) document a 0.96 day year⁻¹ lengthening of the growing season (mostly due to earlier green-up) and a corresponding 0.78% increase in $NDVI$. In their German subdomain (closest to the present study region), the increase is even greater. The present results are not inconsistent with this finding, as the 2003 anomaly in $NDVI$ was positive during spring green-up. In 2003, however, the negative impacts of late-summer drought overwhelmed the positive effects of a warmer spring, leading to a net *reduction* in $NDVI$ integrated over the growing season. If heat waves like that of 2003 become typical in the future European climate, then it is possible that ‘extreme’ events may change the observed trend in $NDVI$ in some portions of Europe, with implications for regional hydrology, agricultural and forestry outlooks, and terrestrial carbon sequestration.

ACKNOWLEDGEMENTS

The authors benefited from discussions with Christoph Schär (ETH Zurich), Xuhui Lee, Jason Evans, and Roland Geerken (Yale University). Evelyne Richard and Jean-Louis Champeaux provided insight on the French landscape. Andre Grenier and Serge Rambal supplied EUROFLUX data. Two anonymous reviewers made useful comments on the manuscript.

This research was supported by NSF/ATM-0112354 and NASA EOS/03-0587-0425.

REFERENCES

- Asrar G, Kanemasu ET, Yoshida M. 1985a. Estimates of leaf-area index from spectral reflectance of wheat under different cultural practices and solar angle. *Remote Sensing of Environment* **17**: 1–11.
- Asrar G, Fuchs M, Kanemasu ET, Hatfield JL. 1984. Estimating absorbed photosynthetic radiation and leaf-area index from spectral reflectance in wheat. *Agronomy Journal* **76**: 300–306.
- Asrar G, Kanemasu ET, Jackson RD, Pinter PJ. 1985b. Estimation of total above-ground phytomass production using remotely sensed data. *Remote Sensing of Environment* **17**: 211–220.
- Bastiaanssen WGM, Menenti M, Feddes RA, Holtslag AAM. 1998a. A remote sensing surface energy balance algorithm for land (SEBAL) – 1. Formulation. *Journal of Hydrology* **213**: 198–212.
- Bastiaanssen WGM, Pelgrum H, Wang J, Ma Y, Moreno JF, Roerink GJ, van der Wal T. 1998b. A remote sensing surface energy balance algorithm for land (SEBAL) – 2. Validation. *Journal of Hydrology* **213**: 213–229.
- Beniston M. 2004. The 2003 heat wave in Europe: A shape of things to come? An analysis based on Swiss climatological data and model simulations. *Geophysical Research Letters* **31**: 2022–2026.
- Betts AK, Ball JH. 1998. FIFE surface climate and site-average dataset 1987–89. *Journal of the Atmospheric Sciences* **55**: 1091–1108.
- Black E, Blackburn M, Harrison G, Hoskins B, Methven J. 2004. Factors contributing to the summer 2003 European heatwave. *Weather* **59**: 217–223.
- Bonn U. 1994. *International Project for The Construction of a Map of the Natural Vegetation of Europe at a Scale of 1:2.5 Million*.
- Bougeault P, Noilhan J, Lacarrere P, Mascart P. 1991. An experiment with an advanced surface parameterization in a mesobeta-scale model. Part 1: implementation. *Monthly Weather Review* **119**: 2358–2373.
- Bounoua L, Collatz GJ, Los SO, Sellers PJ, Dazlich DA, Tucker CJ, Randall DA. 2000. Sensitivity of climate to changes in NDTV. *Journal of Climate* **13**: 277–2292.
- Brubaker KL, Entekhabi D, Eagleson PS. 1993. Estimation of continental precipitation recycling. *Journal of Climate* **6**: 1077–1089.
- Campbell GS, Norman JM. 1998. *An Introduction to Environmental Biophysics*, 2nd edn. Springer-Verlag, New York.
- Chagnon SA. 1968. The La Porte anomaly: Fact or fiction? *Bulletin of the American Meteorological Society* **49**: 4–11.
- Chehbouni A, D. LS, Njuko EG, Monteny BM. 1996. Examination of the difference between radiative and aerodynamic surface temperatures over sparsely vegetated surfaces. *Remote Sensing of Environment* **58**: 177–186.
- Chehbouni A, Lo Seen D, Njuko EG, Lhomme JP, Monteny BM, Kerr YH. 1997. Estimation of sensible heat flux over sparsely vegetated surfaces. *Journal of Hydrology* **188–189**: 855–868.
- Chen F, Pielke RA, Mitchell K. 2001. Land surface hydrology, meteorology, and climate: Observations and modeling. *Water Science and Application*, Vol. 3. American Geophysical Union, Washington D.C.
- Choudhury BJ, Reginato RJ, Idso SB. 1986. An analysis of infrared temperature observations over wheat and calculation of latent heat flux. *Agricultural and Forest Meteorology* **37**: 75–88.
- Ciais P, Reichstein M, Viovy N, Granier A, Ogee J, Allard V, Aubinet M, Buchmann N, Bernhofer C, Carrara A, Chevallier F, De Noblet N, Friend AD, Friedlingstein P, Grunwald T, Heinesch B, Keronen P, Knohl A, Krinner G, Loustau D, Manca G, Matteucci G, Miglietta F, Ourcival JM, Papale D, Pilegaard K, Rambal S, Seufert G, Soussana JF, Sanz MJ, Schulze ED, Vesala T, Valentini R. 2005. Europe-wide reduction in primary productivity caused by the heat and drought in 2003. *Nature* **437**: 529–533.
- Diak GR, Mecikalski JR, Anderson MC, Norman JM, Kustas WP, Torn RD, DeWolf RL. 2004. Estimating land surface energy budgets from space – Review and current efforts at the University of Wisconsin-Madison and USDA-ARS. *Bulletin of the American Meteorological Society* **85**: 65–78.
- Eltahir EAB. 1998. A soil moisture rainfall feedback mechanism I. Theory and observations. *Water Resources Research* **34**: 765–776.
- Eltahir EAB, Bras RL. 1996. Precipitation recycling. *Reviews of Geophysics* **34**: 367–378.
- Farr T, Kobrick M. 2001. The Shuttle Radar Topography Mission. *Eos Transactions-American Geophysical Union* **94**: 583–585.
- Gillespie A, Rokugawa S, Matsunaga T, Cothorn JS, Hook S, Kahle AB. 1998. A temperature and emissivity separation algorithm for Advanced Spaceborne Thermal Emission and Reflection Radiometer (ASTER) images. *IEEE Transactions on Geoscience and Remote Sensing* **36**: 1113–1126.
- Hasager CB, Nielsen NW, Jensen NO, Boegh E, Christensen JH, Dellwik E, Soegaard H. 2003. Effective roughness calculated from satellite-derived land cover maps and hedge-information used in a weather forecasting model. *Boundary-Layer Meteorology* **109**: 227–254.
- Hayden BP. 1998. Ecosystem feedbacks on climate at the landscape scale. *Philosophical Transactions of the Royal Society of London Series B-Biological Sciences* **353**: 5–18.
- Heymann Y, Steenmans C, Croisille G, Bossard M, Lenco M, Wyatt B, Weber J-L, O'Brian C, Cornaert M-H, Sifakis N. 1993. Environment, Nuclear safety and Civil protection series. CORINE Land Cover: Technical Guide. Commission of the European Communities, Office for Official Publications of the European Communities: Luxembourg, Report number: EUR 12585, 144.
- Housego K. 2003. France turns attention to farmers devastated in heat wave. In *The Associated Press*, BC cycle (ed). <http://www.sfgate.com/cgi-bin/article.cgi?f=/news/archive/2003/08/22/international0640EDT0483.DTL> [Accessed 12 November 2005].
- Huete A, Justice CO, van Leeuwen W. 1999. *MODIS vegetation product (MOD13)*, Version 3, 129.
- INSEE. 2004. *L'agriculture en 2003 en Europe et en France; Les grands pays agricoles affectés par la secheresse* Number 974, 4.
- Jacob F, Olioso A, Gu XF, Su ZB, Seguin B. 2002. Mapping surface fluxes using airborne visible, near infrared, thermal infrared remote sensing data and a spatialized surface energy balance model. *Agronomie* **22**: 669–680.
- Ji L, Peters AJ. 2003. Assessing vegetation response to drought in the northern Great Plains using vegetation and drought indices. *Remote Sensing of Environment* **87**: 85–98.
- Kalnay E, Kanamitsu M, Kistler R, Collins W, Deaven D, Gandin L, Iredell M, Saha S, White G, Woollen J, Zhu Y, Chelliah M, Ebisuzaki W, Higgins W, Janowiak J, Mo KC, Ropelewski C, Wang J, Leetmaa A, Reynolds R, Jenne R, Joseph D. 1996. The NCEP/NCAR 40-year reanalysis project. *Bulletin of the American Meteorological Society* **77**: 437–471.
- Kogan FN. 1995. Application of vegetation index and brightness temperature for drought detection. *Natural Hazards: Monitoring and Assessment Using Remote Sensing Technique* 91–100. *Advances in Space Research* **15/11**: Pergamon Press, Oxford.

- Kogan FN. 1997. Global drought watch from space. *Bulletin of the American Meteorological Society* **78**: 621–636.
- Liou KN. 2002. *An Introduction to Atmospheric Radiation, International Geophysics Series*, 2nd edn. Vol. 84. Academic Press, San Diego.
- Liu WT, Kogan FN. 1996. Monitoring regional drought using the vegetation condition index. *International Journal of Remote Sensing* **17**: 2761–2782.
- Mahrt L, Vickers D. 2004. Bulk formulation of the surface heat flux. *Boundary-Layer Meteorology* **110**: 357–379.
- Meehl GA, Tebaldi C. 2004. More intense, more frequent, and longer lasting heat waves in the 21st century. *Science* **305**: 994–997.
- Myneni RB, Williams DL. 1994. On the relationship between Fapar and Ndvi. *Remote Sensing of Environment* **49**: 200–211.
- Noilhan J, Lacarrere P, Bougeault P. 1991. An Experiment with an advanced surface parameterization in a Mesobeta-Scale Model. 3. Comparison with the Hapex-Mobilhy Dataset. *Monthly Weather Review* **119**: 2393–2413.
- Norman JM, Divakarla M, Goel NS. 1995. Algorithms for extracting information from remote thermal-IR observations of the Earth's atmosphere. *Remote Sensing of Environment* **51**: 157–168.
- Painho M. 1996. Digital Map of European Ecological Regions (DMEER): its concept and elaboration. *Second Joint European Conference & Exhibition on Geographical Information*, Barcelona.
- Peters AJ, Walter-Shea EA, Ji L, Vina A, Hayes M, Svoboda MD. 2002. Drought monitoring with NDVI-based standardized vegetation index. *Photogrammetric Engineering and Remote Sensing* **68**: 71–75.
- Pielke RA. 2001. Influence of the spatial distribution of vegetation and soils on the prediction of cumulus convective rainfall. *Reviews of Geophysics* **39**: 151–177.
- Pielke RA, Avissar R. 1990. Influence of landscape structure on local and regional climate. *Landscape Ecology* **4**: 133–155.
- Pielke RA, Dalu GA, Snook JS, Lee TJ, Kittel TGF. 1991. Nonlinear influence of mesoscale land use on weather and climate. *Journal of Climate* **4**: 1053–1069.
- Räisänen J, Hansson U, Ullerstig A, Doscher R, Graham LP, Jones C, Meier HEM, Samuelsson P, Willen U. 2004. European climate in the late twenty-first century: Regional simulations with two driving global models and two forcing scenarios. *Climate Dynamics* **22**: 13–31.
- Rasmussen MS. 1998. Developing simple, operational, consistent NDVI-vegetation models by applying environmental and climatic information: Part I. Assessment of net primary production. *International Journal of Remote Sensing* **19**: 97–117.
- Schaaf CB, Gao F, Strahler AH, Lucht W, Li X, Tsang T, Strugnell NC, Zhang X, Jin Y, Muller J-P, Lewis P, Barnsley M, Hobson P, Disney M, Roberts G, Dunderdale M, Doll C, d'Entremont R, Hu B, Liang S, Privette JL. 2002. First operational BRDF, albedo, and nadir reflectance products from MODIS. *Remote Sensing of Environment* **83**: 135–148.
- Schär C, Jendritzky G. 2004. Climate change: Hot news from summer 2003. *Nature* **432**: 559–560.
- Schär C, Luthi D, Beyerle U, Heise E. 1999. The soil-precipitation feedback: A process study with a regional climate model. *Journal of Climate* **12**: 722–741.
- Schär C, Vidale PL, Luthi D, Frei C, Haberli C, Liniger MA, Appenzeller C. 2004. The role of increasing temperature variability in European summer heatwaves. *Nature* **427**: 332–336.
- Shukla J, Nobre C, Sellers PJ. 1990. Amazon deforestation and climate change. *Science* **247**: 1322–1325.
- Small EE, Kurc SA. 2003. Tight coupling between soil moisture and the surface radiation budget in semiarid environments: Implications for land-atmosphere interactions. *Water Resources Research* **39**: 1278–1291.
- Stöckli R, Vidale PL. 2004. European plant phenology and climate as seen in a 20-year AVHRR land-surface parameter dataset. *International Journal of Remote Sensing* **25**: 3303–3330.
- Sugita M, Brutsaert W. 1990. Regional surface fluxes from remotely sensed skin temperature and lower boundary layer measurements. *Water Resources Research* **26**: 2937–2944.
- Trenberth KE. 1999. Atmospheric moisture recycling: Role of advection and local evaporation. *Journal of Climate* **12**: 1368–1381.
- Tucker CJ, Justice CO, Prince SD. 1986. Monitoring the grasslands of the Sahel 1984–1985. *International Journal of Remote Sensing* **7**: 1571–1581.
- Vermote EF, Vermeulen A. 1999. *Atmospheric Correction Algorithm: Spectral Reflectances (MOD09)*, Version 4.0, US National Aeronautics and Space Administration, Greenbelt MD, 108.
- Veroustraete F, Sabbe H, Eerens H. 2002. Estimation of carbon mass fluxes over Europe using the C-Fix model and Euroflux data. *Remote Sensing of Environment* **83**: 376–399.
- Vidale PL, Luthi D, Wegmann R, Schär C. 2006. European climate variability in a heterogeneous multi-model ensemble. *Climatic Change*. accepted.
- Wan Z, Wang P, Li X. 2004. Using MODIS land surface temperature and normalized difference vegetation Index products for monitoring drought in the southern Great Plains, USA. *International Journal of Remote Sensing* **25**: 61–72.
- Zhou L, Kaufmann RK, Tian Y, Myneni RB, Tucker CJ. 2003. Relation between interannual variations in satellite measures of northern forest greenness and climate between 1982 and 1999. *Journal of Geophysical Research* **108**: 31–37.
- Zhou L, Tucker C, Kaufmann R, Slayback D, Shabanov N, Myneni R. 2001. Variations in northern vegetation activity inferred from ACL satellite data of vegetation index during 1981 to 1999. *Journal of Geophysical Research* **106**: 20069–20083.